

**FACTORS CONTROLLING WATER RETENTION OF ALLUVIAL DEPOSITS,  
WESTERN MOJAVE DESERT**

A Thesis

Presented to

The Department of Geology

San Jose State University

In Partial Fulfillment

Of the Requirements for the Degree

Master of Science

by

Kari A. Winfield

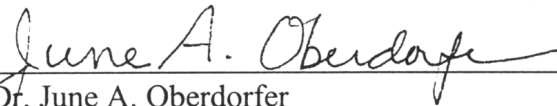
December 2000

© 2000

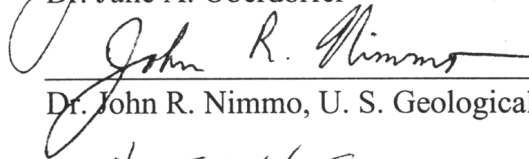
Kari A. Winfield

All Rights Reserved

APPROVED FOR THE DEPARTMENT OF GEOLOGY



Dr. June A. Oberdorfer

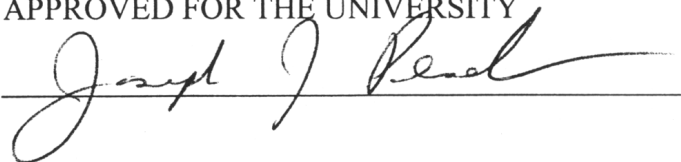


Dr. John R. Nimmo, U. S. Geological Survey



Dr. David W. Andersen

APPROVED FOR THE UNIVERSITY



## ABSTRACT

### FACTORS CONTROLLING WATER RETENTION OF ALLUVIAL DEPOSITS, WESTERN MOJAVE DESERT

by Kari A. Winfield

Water-retention curves were measured on undisturbed core samples of gravelly sand, collected from boreholes or channel walls at Oro Grande Wash and Sheep Creek Wash, located in the western Mojave Desert, California. Trends among retention properties (median pore size, pore-size sorting, air-entry pressure, and porosity) and bulk core properties (median particle size, particle-size sorting, grain arrangement, and stratification) were examined for structural and textural effects. Textural effects overwhelmed structural effects. Effects due to stratification were insignificant for the degree of textural contrast between layers in the cores. Insufficient information was available to determine the effect of grain arrangement, arising from differing styles of deposition. Median particle size correlated strongly with median pore-size and air-entry pressure, whereas particle-size sorting was found to be the main control on porosity and, to a lesser degree, air-entry pressure.

## ACKNOWLEDGMENTS

I would like to thank the U. S. Geological Survey and the Mojave Water Agency for providing funding for this project. In particular, my appreciation is extended to John Izbicki and John Nimmo of the U. S. Geological Survey for initiating this research and for their guidance and support during this work. Also my gratitude is given to the faculty members at San Jose State University, whose expertise in geology and excellent teaching skills have enabled me to progress far.

## TABLE OF CONTENTS

	Page
INTRODUCTION.....	1
Water Retention.....	1
Study Objectives .....	9
SITE DESCRIPTION .....	11
Oro Grande Wash.....	11
Sheep Creek Wash .....	13
SAMPLE COLLECTION.....	17
Drill Core Samples.....	17
Surface Core Samples .....	18
EXPERIMENTAL METHODS.....	21
Wetting Solution .....	21
Sample Saturation .....	23
Water-Retention Curves.....	23
Controlled Liquid-Volume Method .....	23
General .....	23
Equipment .....	24
Procedure.....	24
Filter Paper Method and Forced Evaporation of Water .....	28
General .....	28

Procedure.....	28
Bulk Properties.....	30
Core Extraction and Description.....	30
Oven-Dryness.....	30
Porosity.....	30
Particle Size.....	31
METHODS OF DATA ANALYSIS .....	33
Water-Retention Data.....	33
Empirical Curve Fits to Measured Data.....	33
Calculation of Pore-Size Distributions.....	35
Textural Classification .....	37
Graphical Statistics.....	37
RESULTS.....	39
Bulk Properties.....	39
Core Description .....	39
Particle-Size Distributions and Statistics .....	41
Water-Retention Properties.....	44
Pore-Size Distributions and Statistics .....	46
ERROR ANALYSIS.....	49
Experimental Errors .....	49
Matric Pressure Head Errors .....	49
Water Content Errors .....	52

Particle-Size Errors .....	53
Errors in Data Analysis .....	54
Empirical Curve Fits .....	54
Calculation of Pore-Size Distributions.....	55
DISCUSSION OF RESULTS.....	56
Bulk Physical Properties .....	56
Hydraulic Properties.....	61
Comparison of Bulk and Hydraulic Properties .....	62
Sensitivity of Interpretations to Curve-Fit Procedure .....	74
Recommendations for Future Studies .....	80
CONCLUSIONS.....	83
REFERENCES CITED.....	85



## LIST OF ILLUSTRATIONS

Figure	Page
1. Location of Study Areas.....	2
2. Textural Effects on Water-Retention Curves.....	5
3. Idealized Cross-Sections of Sedimentary Structure.....	6
4. Hypothetical Structural Effects on Water-Retention Curves.....	7
5. Areal Extent of Victorville Fan and Sheep Creek Fan Deposits.....	12
6. Fluvial Deposits at Oro Grande Wash.....	14
7. Debris-Flow Deposits at Sheep Creek Wash.....	16
8. Method of Surface Core Collection.....	19
9. Laboratory Apparatus.....	22
10. Example Output Record from the Pressure Transducer.....	26
11. Sketches of Core Structure.....	40
12. Particle-Size Distributions.....	42
13. Particle-Size Histograms.....	43
14. Water-Retention Curves.....	45
15. Pore-Size Histograms.....	47
16. Classification Scheme Based on Particle-Size Sorting and Stratification.....	57
17. Particle-Size Sorting Versus Particle-Size Skewness.....	60
18. Pore- and Particle-Size Histograms for Samples of Type 1 and Type 2.....	63
19. Pore- and Particle-Size Histograms for Samples of Type 3.....	64

20. Pore- and Particle-Size Histograms for Samples of Type 3 or 4 and Type 4 .....	65
21. Trends in Pore-Size Sorting and Median Pore Radius.....	67
22. Trends in the Ratio of the Particle- to Pore-Size Median .....	69
23. Trends in the Air-Entry Pressure.....	71
24. Trends in Porosity .....	72
25. Sensitivity of Pore-Size Sorting to Curve-Fit Procedure .....	79

## LIST OF TABLES

Table	Page
1. Sample Depth and Location .....	17
2. Example Calculation of Volumetric Water Contents.....	27
3. Bulk Properties .....	39
4. Textural Classification .....	41
5. Particle-Size Statistics.....	44
6. van Genuchten Parameters with Calculated $\Phi$ and Optimized $\theta_r$ .....	46
7. Pore-Size Statistics for Curve Fits Using Calculated $\Phi$ and Optimized $\theta_r$ .....	48
8. Sample Classification Based on Particle-Size Sorting and Stratification .....	58
9. Bulk Physical and Hydraulic Properties Related to Structural and Textural Trends between Samples .....	66
10. van Genuchten Parameters with Calculated $\Phi$ and $\theta_r = 0$ .....	76
11. Pore-Size Statistics for Curve Fits Using Calculated $\Phi$ and $\theta_r = 0$ .....	76
12. van Genuchten Parameters with Measured $\theta_{sat}$ and Optimized $\theta_r$ .....	77
13. van Genuchten Parameters with Measured $\theta_{sat}$ and $\theta_r = 0$ .....	77

## INTRODUCTION

This study is part of a larger joint project between the U. S. Geological Survey and the Mojave Water Agency to determine natural recharge rates to the regional aquifer in the western Mojave Desert. Several washes have been considered to estimate natural recharge and as sites to focus artificial recharge, including Sheep Creek Wash and Oro Grande Wash (Fig. 1). Since population in the Victorville area has more than tripled from 90,000 in 1980 to greater than 270,000 in 1995 (Izbicki and others, 1995), water demands have also increased as the regional aquifer has been stressed due to increased pumping. In order to understand important issues of arid-region hydrology, such as aquifer recharge and contaminant migration, the basic unsaturated hydraulic properties must be characterized. This includes determining hydraulic conductivity as a function of water content,  $K(\theta)$ , and water retention, or water content as a function of matric pressure head,  $\theta(\psi)$ . With a better understanding of how these unsaturated hydraulic properties are affected by characteristics of the geologic medium, such as sedimentary texture, structure, mineralogy, and stratification, the accuracy of unsaturated flow models and estimates of recharge can be improved.

### Water Retention

Water retention,  $\theta(\psi)$ , is generally easier to measure than hydraulic conductivity, reflects physical properties of the soil or sediment, and is needed in unsaturated flow models to estimate recharge. Conceptual models of water retention often assume that

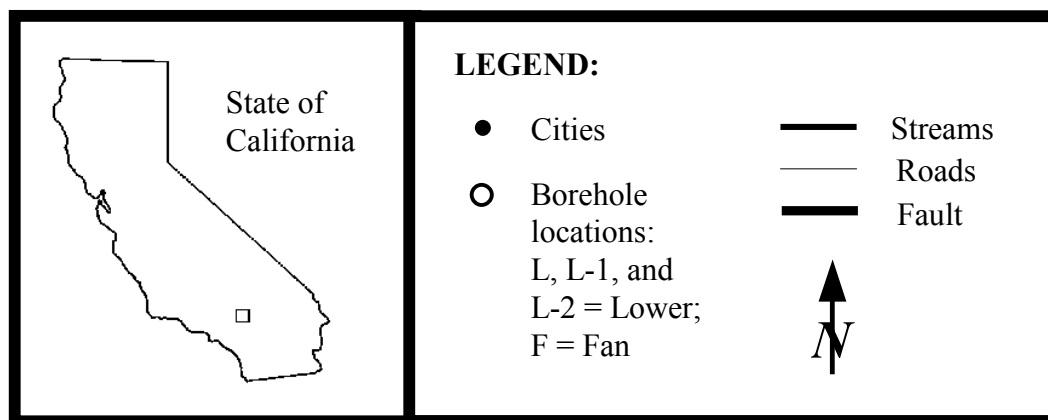
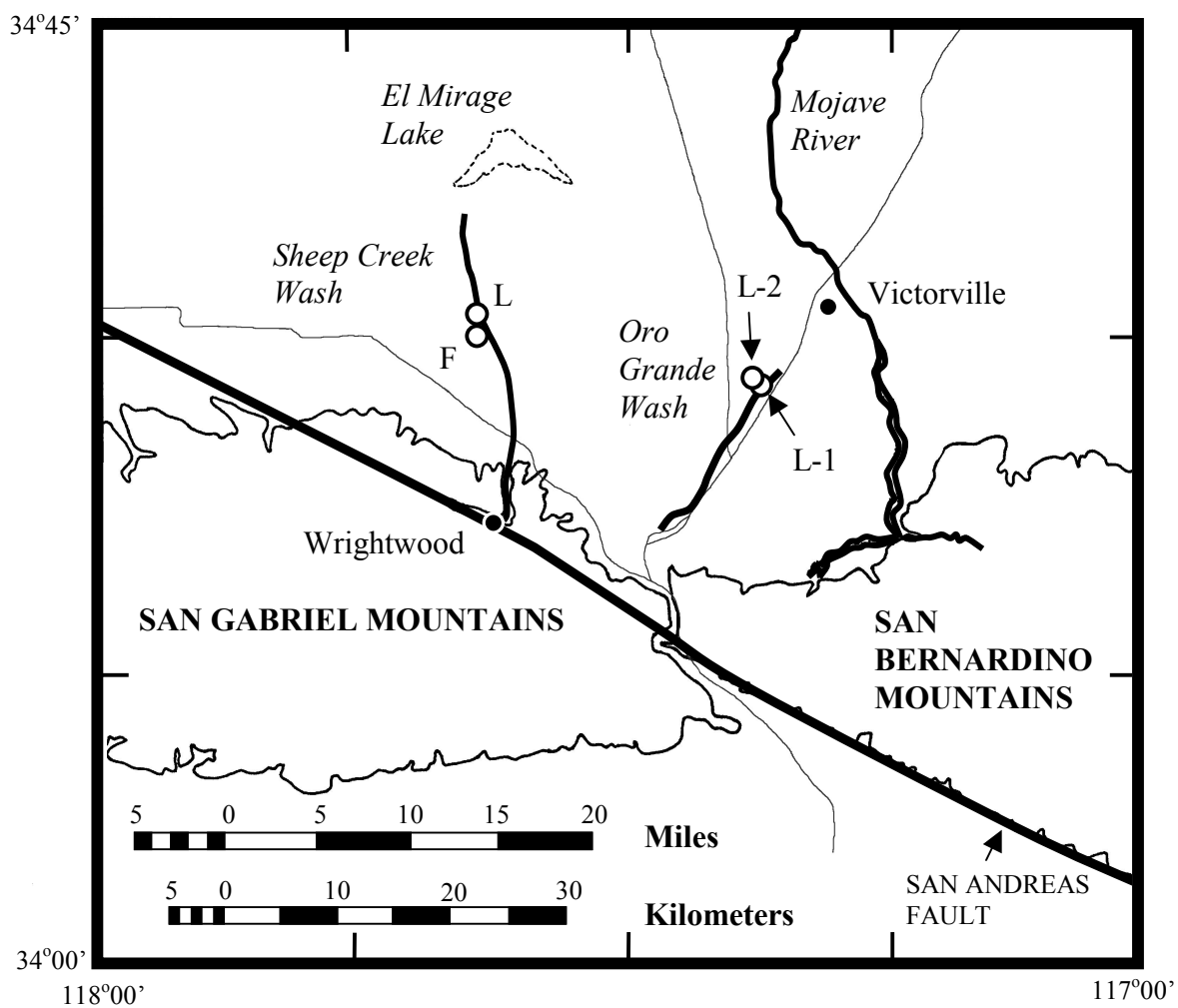


Figure 1. Location of the two study areas, Sheep Creek Wash and Oro Grande Wash, in the western Mojave Desert, California (adapted from U. S. Geological Survey, 1:250,000 San Bernardino quadrangle).

pores can be approximated by a bundle of capillary tubes. According to capillary theory, the matric pressure head,  $\psi$ , relates to the effective pore radius,  $R$ , by:

$$\psi = -2\sigma\cos(\delta)/\rho gR,$$

where:  $\sigma$  = surface tension of the air-water interface

$\delta$  = contact angle of water with the pore wall

$\rho$  = density of water

$g$  = acceleration due to gravity

Because  $\psi$  and  $R$  are inversely related, large pores are associated with smaller magnitudes of matric pressure head (less negative values). The largest pores determine the air-entry value of the soil,  $\psi_{ae}$ , the pressure at which drainage begins during desaturation. Using the capillary model, the pore-size distribution of a soil can be calculated directly from the  $\theta(\psi)$  function. Each measured  $\psi$  value is converted to an effective pore radius at its associated water content and each measured  $\theta$  value is normalized to porosity. This conversion assumes that the surface tension of the pore water is uniform throughout the sample and that temperature effects are negligible. For wettable materials, the contact angle,  $\delta$ , is small and is often assumed to be zero.

Water retention is influenced both by the texture and by the structure of the geologic medium. Whereas texture refers to the particle-size distribution of the soil, structure refers to the packing arrangement of the soil components resulting from natural depositional sorting, aggregate formation, or the presence of macropores created by roots, animal burrows, or shrink/swell phenomena. Stratification may also be considered a

structural feature, involving textural contrasts between layers, differences in intralayer grain sorting, or both. The textural component of retention is most often measured in soil physics when a sample is repacked, destroying the natural structure. The textural influence upon retention is readily observed (Fig. 2), assuming structural effects are negligible. Fine-textured soils (e.g., clays) have finer pore-size distributions than coarse-textured soils (e.g., sands or gravels). As a result, clays retain more water than sands for a given matric pressure head value. Also, the air-entry value of a fine-textured soil, due to its higher percentage of small pores, is lower (more negative) than that of a coarse-textured soil.

Structural effects on water retention are less well known and are often ignored in attempts to model retention. The natural deposition of particles of varying sizes can produce a relatively random sedimentary structure, as in a debris flow, or a more ordered structure, as in a normally graded stream deposit. In a normally graded fluvial deposit, consisting of multiple, well-sorted layers, large pores are created between adjacent large particles. In a debris-flow deposit, whether well stratified or not, these large pores are absent, with the spaces next to large particles being occupied by smaller grains (Fig. 3). A fluvial sample consisting of multiple well-sorted layers is expected to have a wide range of pore sizes, reflected by a more gentle drainage slope (Fig. 4), due to the greater presence of both large and small pores. A debris-flow sample of similar texture would tend to have a narrower pore-size distribution, arising from the random arrangement of the particles, tighter packing geometry, and lack of large pores next to large particles. To capture multiple layers within a sample, the sample size must be large relative to the

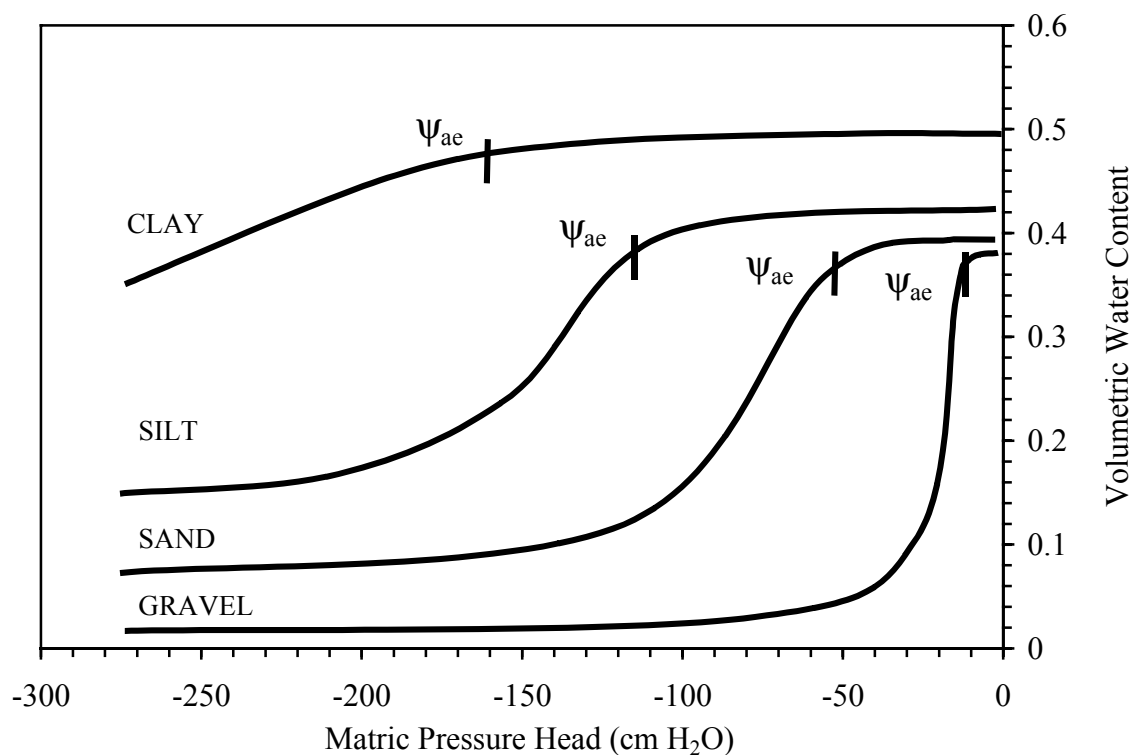


Figure 2. Textural effects on hypothetical water-retention curves (modified from Stephens, 1996). More finely textured soils, such as clays, yield lower matric pressure values ( $\psi$ ) and have lower air-entry values ( $\psi_{ae}$ ) for a given water content ( $\theta$ ) than coarse-grained soils, such as sands or gravels.



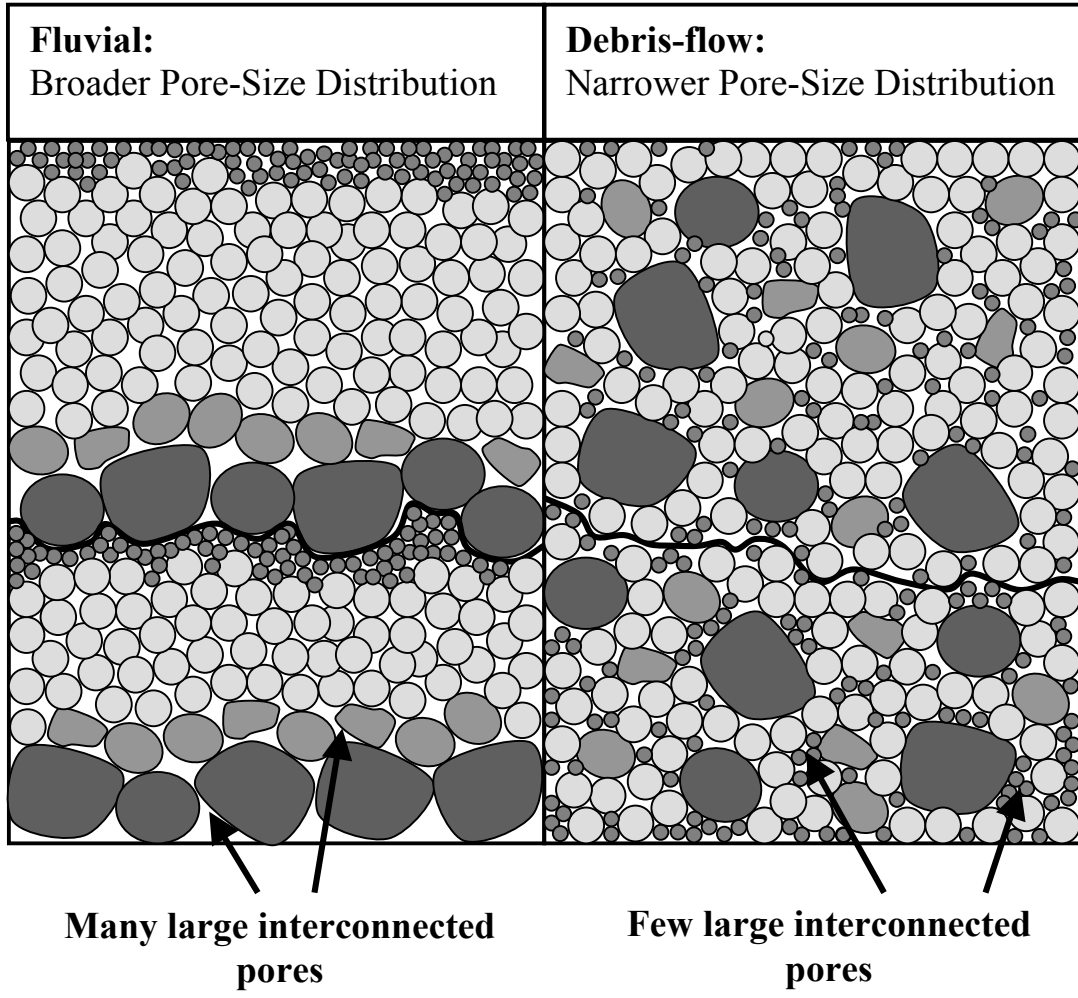


Figure 3. Idealized cross-sections of sedimentary structure for a fluvial deposit and a debris-flow deposit.

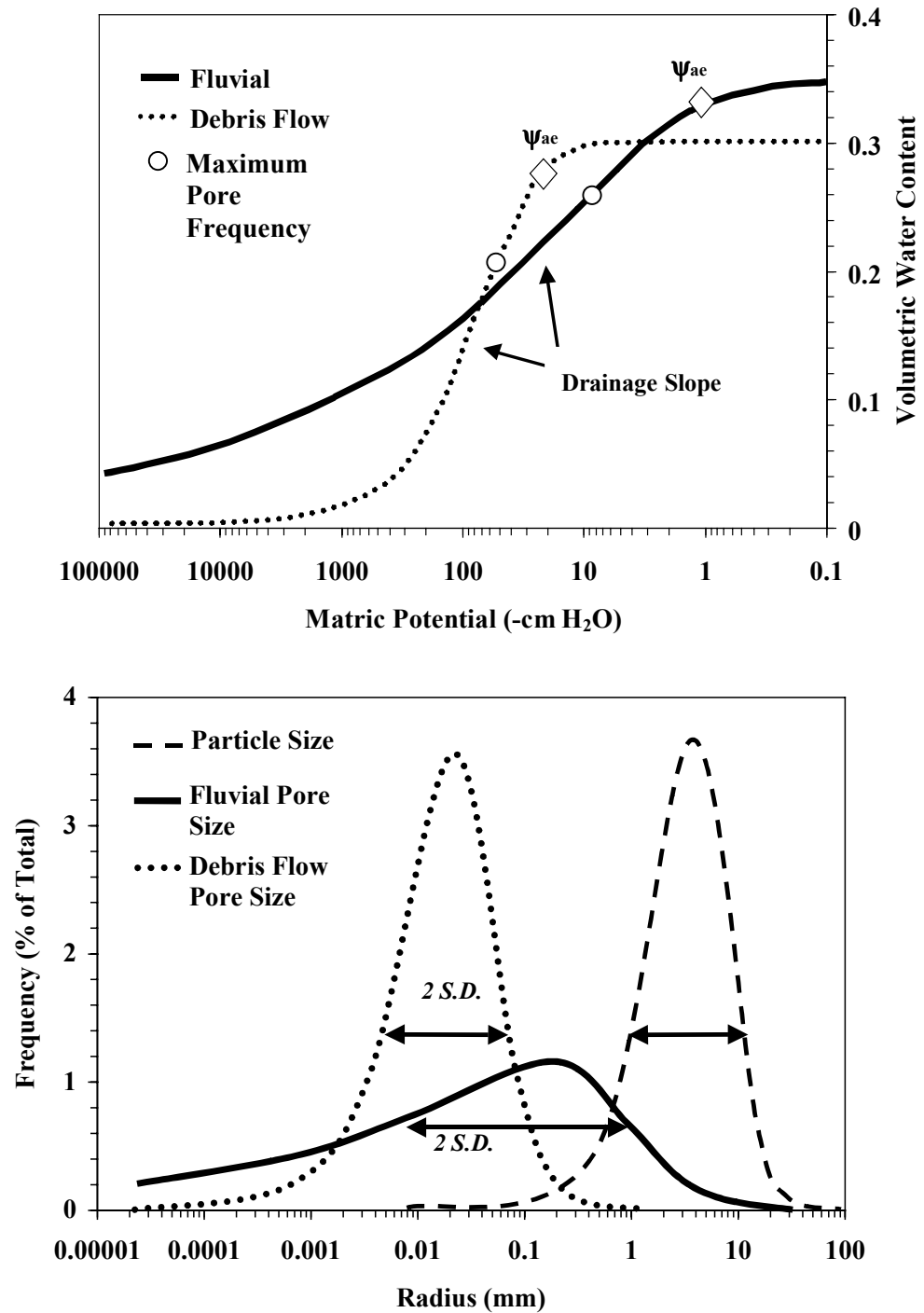


Figure 4. Hypothetical structural effects on water-retention curves (upper diagram) for a fluvial and a debris-flow deposit. The lower diagram shows pore-size distributions calculated from these retention curves using capillary theory.

thickness of the layers. Samples collected from thinly stratified deposits may encompass multiple layers, whereas samples collected from deposits with thicker beds may only capture one or two layers or even a partial layer. Therefore, stratification, in addition to particle-size sorting, needs to be examined for each sample. A fluvial sample with a broad pore-size distribution would be expected to have a higher (less negative) air-entry pressure than a debris-flow sample of similar texture (Fig. 4). As a result of their random orientation and packing arrangement, particles in a debris-flow sample should pack more closely than particles in a fluvial sample. The bulk density, or calculated porosity, of a debris-flow sample is therefore expected to be lower than that of a fluvial sample of comparable particle-size distribution.

Due to the time required for direct measurement of retention and the abundance of soil survey data, workers have attempted to model retention from basic physical properties such as organic matter content, porosity, particle-size distribution, and aggregate-size distribution (e.g., Gupta and Larson, 1979; Arya and Paris, 1981; Haverkamp and Parlange, 1986; Nimmo, 1997). Comparisons of modeled results to measured retention points showed variable degrees of agreement, likely because the models were tested on small data sets, for particular textural classes, or on repacked samples. The model of Arya and Paris (1981) requires particle-size distribution and porosity as inputs, but excludes any measure of structure. Nimmo (1997) modified this model to include structure, specifically macropores and aggregate-size distribution, which improved the agreement between modeled and measured retention values. Further study is needed, on larger and more diverse data sets, before water retention can be

predicted from other soil properties with a high degree of confidence.

Even though textural influences on retention are well known, there have been few studies that investigate the effect of structure on retention. Physico-empirical models of retention, including the one presented by Arya and Paris (1981), rely on easily measured bulk properties, such as particle-size distributions and porosity, to provide the necessary information for prediction of retention. However, the addition of structural information may be needed to accurately predict retention properties from a small number of physically measured properties.

### Study Objectives

The main purpose of this study is to determine what factors control the water-retention properties of sediments from two arid-region washes with different depositional histories. Along incised portions of Oro Grande Wash, the deposits appear to be dominantly fluvial in nature, whereas Sheep Creek Wash appears to be debris-flow dominated. Core samples are categorized on the basis of stratification and particle-size sorting, to attempt to differentiate between debris flow or fluvial structure.

Controlling factors are related to texture or structure. Textural factors include information obtained from the particle-size distributions, such as mean or median particle size and particle-size sorting, whereas structural factors, including grain arrangement and stratification, are observed from the cores themselves. This study compares specific retention properties, including the air-entry pressure, porosity, the range of pore sizes (pore-size sorting), and the median pore size, with bulk physical properties of the

samples. Bulk properties include median particle size and particle-size sorting. The identification of controlling factors is needed for refining models of retention, unsaturated flow models, and estimation of recharge.

The results of this study provide accurate water-retention data for use in the unsaturated-flow model VS2D (Lappala and others, 1987), which will be implemented by scientists at the U. S. Geological Survey. Previous attempts to measure  $K(\theta)$  at Sheep Creek Wash were unsuccessful due the friable nature of the core samples, resulting from low field water contents. The information from this study may aid in relating the unsaturated hydraulic properties of materials without prior  $K(\theta)$  measurements to ones with previous measurements, depending on whether textural or structural effects dominate the retention properties.

## SITE DESCRIPTION

The study area consists of two sites, Oro Grande Wash and Sheep Creek Wash, which comprise part of the upper Mojave River basin of the western Mojave Desert (Figs. 1 and 5). Both are ephemeral streams that drain northward from the eastern San Gabriel Mountains of the greater Transverse Range province. The unsaturated zone in this area ranges in thickness from 400 m near the mountain front to 70 m towards the basin. The gradient of the ground-water table is approximately 0.4 % and trends toward the northeast. Precipitation in the area is less than 15 cm/yr, and is highest near the mountain front (Izbicki and others, 1998). The San Andreas fault passes through the headwater regions of these streams along the northern margin of the San Gabriel Mountains.

### Oro Grande Wash

Oro Grande Wash, an ephemeral tributary to the Mojave River, has a drainage area of 72 km<sup>2</sup> (27.8 mi<sup>2</sup>) and an average channel width of 0.4 m (1.2 ft). The estimated mean annual discharge is 49,340 m<sup>3</sup> (40 acre-ft) with an estimated runoff of 0.8 mm (0.03 in) (Lines, 1995). The average gradient of the stream is 2.5 % (130 ft/mile), as measured from the 1:100,000 Victorville and San Bernardino quadrangles (U.S. Geological Survey).

The recent channel fill of Oro Grande Wash consists mainly of reworked fan deposits. The older sediments adjacent to and underlying the fill are part of the

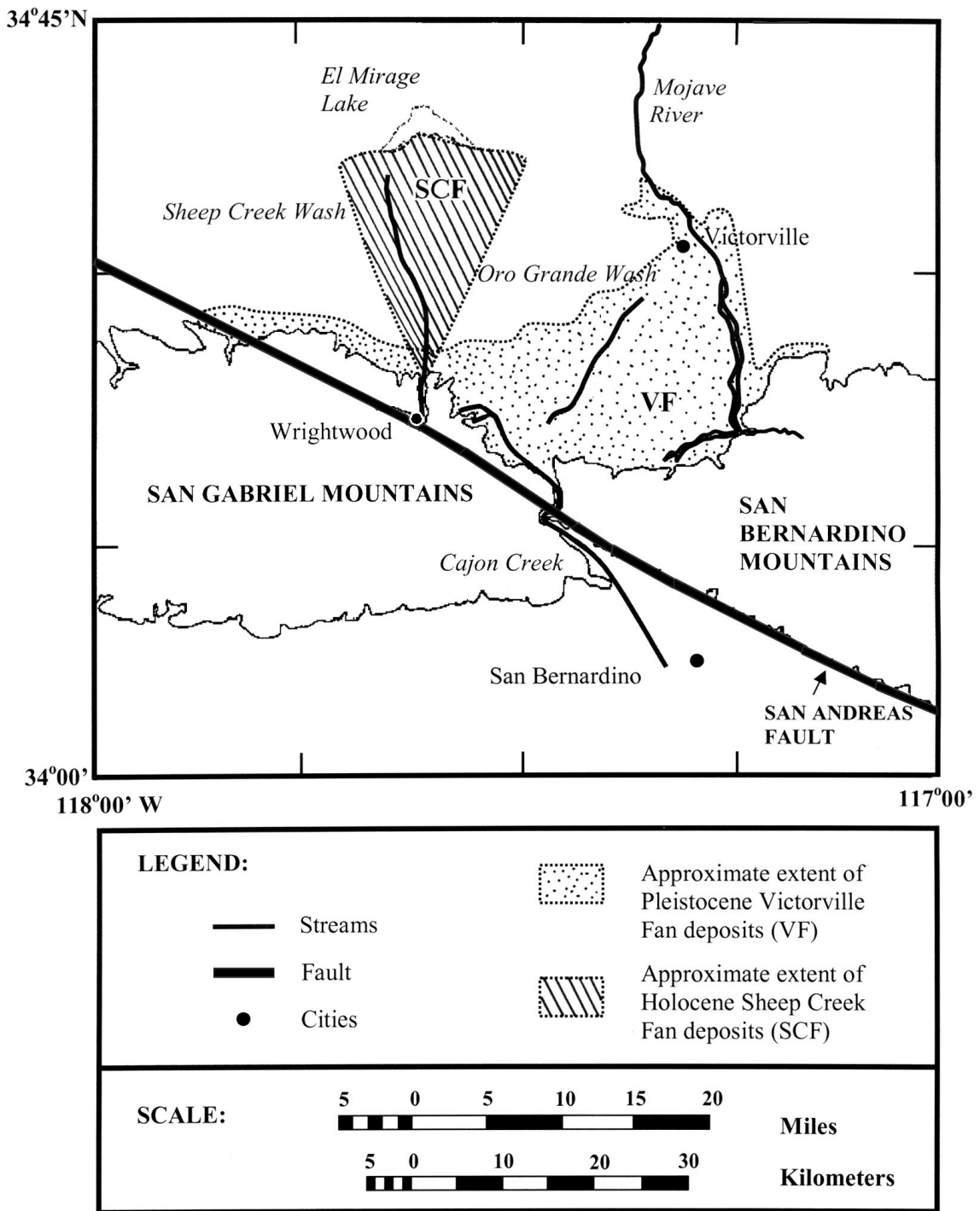


Figure 5. Areal extent of the Victorville fan and the Sheep Creek fan deposits (modified from Weldon, 1985).

Victorville Fan Complex (Fig. 5), a system of coalesced fans that were shed northward off the San Gabriel Mountains beginning about 1.5 Ma (Weldon, 1985; Meisling and Weldon, 1989). With movement along the San Andreas fault, headward erosion of the south-flowing Cajon Creek has beheaded the active fan complex. The source rocks for the Victorville fan deposits consist of schist, granodiorite, and sandstone, which reflect the changing source area as the southern block of the San Andreas moved northwestward (Meisling and Weldon, 1989).

Because the high source area has been removed by stream capture, parts of the wash have incised into the fan surface in order to reach the new base-level of the Mojave River, which lies about 1.5 km to the northeast of the lower part of the wash. Sediments along the channel walls near the lower borehole, L-1 (Fig. 1), appear to be dominantly fluvial in character, with abundant cross-bed sets and gravel lenses, perhaps reflecting a braided stream environment (Fig. 6).

### Sheep Creek Wash

Sheep Creek Wash is the current trunk stream of the Sheep Creek fan (Fig. 5), whose source area is located in the San Gabriel Mountains near the town of Wrightwood. Source rocks include, primarily, a muscovite-quartz-garnet schist, known as the Pelona Schist, and, to a lesser degree, granite. The Pelona Schist is highly foliated and landslide-prone, and is associated with debris flows and mudflows that have affected the town of Wrightwood (Sharp and Nobles, 1953; Morton and Sadler, 1989). The relief of the source area ranges from 120 to 300 m (400 to 1000 ft). The total length of the wash is





Figure 6. Fluvial deposits, including gravel lenses and cross-stratification, observed along the eastern channel wall of Oro Grande Wash near borehole L-1. Lens cap is 52 mm in diameter.

approximately 30 km, with a gradient of 4.9 % (250 ft/mile) in the headwater region and 0.3 % (110 ft/mile) along the middle to lower fan surface. The axial length of the fan along the surface is approximately 24 km (15 miles), with the distal portions extending as far as El Mirage Lake (U.S. Geological Survey, 1:100,000 Victorville and San Bernardino quadrangles). The fan is younger (Holocene) than the Victorville Fan Complex (Pleistocene) and appears to be debris-flow dominated along incised portions of the wash (Fig. 7). The incision of the wash may have resulted from uplift of the San Gabriel Mountains during the deposition of the fan sediments.



Figure 7. Example of debris-flow deposits along the western channel wall of Sheep Creek Wash, near the lower (L) borehole. Lens cap is 52 mm in diameter.

## SAMPLE COLLECTION

Large (10-cm diameter by 15-cm length) drill core and surface core samples were collected near the lower reaches of Sheep Creek Wash and Oro Grande Wash. For each sample used in this study, Table 1 includes information on depth of sampling and location of the nearest borehole (L-1 and L refer to boreholes drilled at the lower reaches of the washes, directly in the channels; L-2 and F refer to boreholes drilled on the adjacent fan surfaces). The sample designation, drill core (D) or surface sample (S), is also given.

Table 1. Sample Depth and Location

Sample		Depth		Location	Sample Type
		m	ft	Nearest Hole <sup>1</sup>	D or S <sup>2</sup>
Oro Grande Wash	OGW-1	~1.5	~5	L-1	S
	OGW-2	~2.4	~8	L-1	S
	OGW-4	~4	~13	L-1	S
	OGL 11.5-12	3.5	11.5	L-1	D
	LOGW-2 82-82.5	25	82	L-2	D
Sheep Creek Wash	SCW-1	~0.9	~3	L	S
	SCW-2	~0.6	~2	L	S
	SCW-4	~0.6	~2	L	S
	SCF 57-57.5	17.4	57	F	D
	LSCW 58-58.5	17.7	58	L	D

<sup>1</sup>Borehole locations are shown in Figure 1. L and L-1 refer to boreholes drilled directly into the channels at their lower reaches. L-2 and F refer to boreholes drilled into the adjacent fan surfaces.

<sup>2</sup>D = drill core sample; S = surface sample.

### Drill Core Samples

Core samples were collected from boreholes drilled by the U. S. Geological Survey in 1994, 1995, and 1997 (Fig. 1) to depths of approximately 30 m below land surface. Four 15-cm- (6-in-) long cores were obtained at every 1.3 m depth by piston-

core barrel in either 9- or 10-cm- (3.5- or 4-in-) diameter aluminum or brass liners (Izbicki and others, 1995; 1998; Izbicki, 1999). Only the 10-cm-diameter cores were used in this study due to limitations of the experimental design. The ODEX air-hammer method (Driscoll, 1986) prevented contamination by drilling fluids. After collection cores were immediately capped, sealed with electrical tape, wrapped in plastic, and enclosed in heat-sealed aluminum pouches in order to preserve field moisture conditions (Izbicki and others, 1998). Drill core samples used for this study, including depth and location, are listed in Table 1.

#### Surface Core Samples

In July 1998, surface samples were collected along incised parts of the channels, using a technique that did not require expensive or highly technical equipment and that allowed use of the original core liners (10-cm diameter by 15-cm length). The choice of sampling locations depended on the apparent texture of the sediments and the depositional environment, with the requirement that the location be representative of the dominant depositional environment for each wash. After creation of a bench in the channel wall, the liner was placed on the resulting horizontal surface. To aid in sampling and cohesion, water was added to the top of the liner and allowed to percolate downward. Sediment was then carved from around the base, creating a pedestal, and the liner was pushed downward (Fig. 8). This process was repeated until the liner was completely filled. Cores were capped and sealed with electrical tape after collection to prevent evaporation.

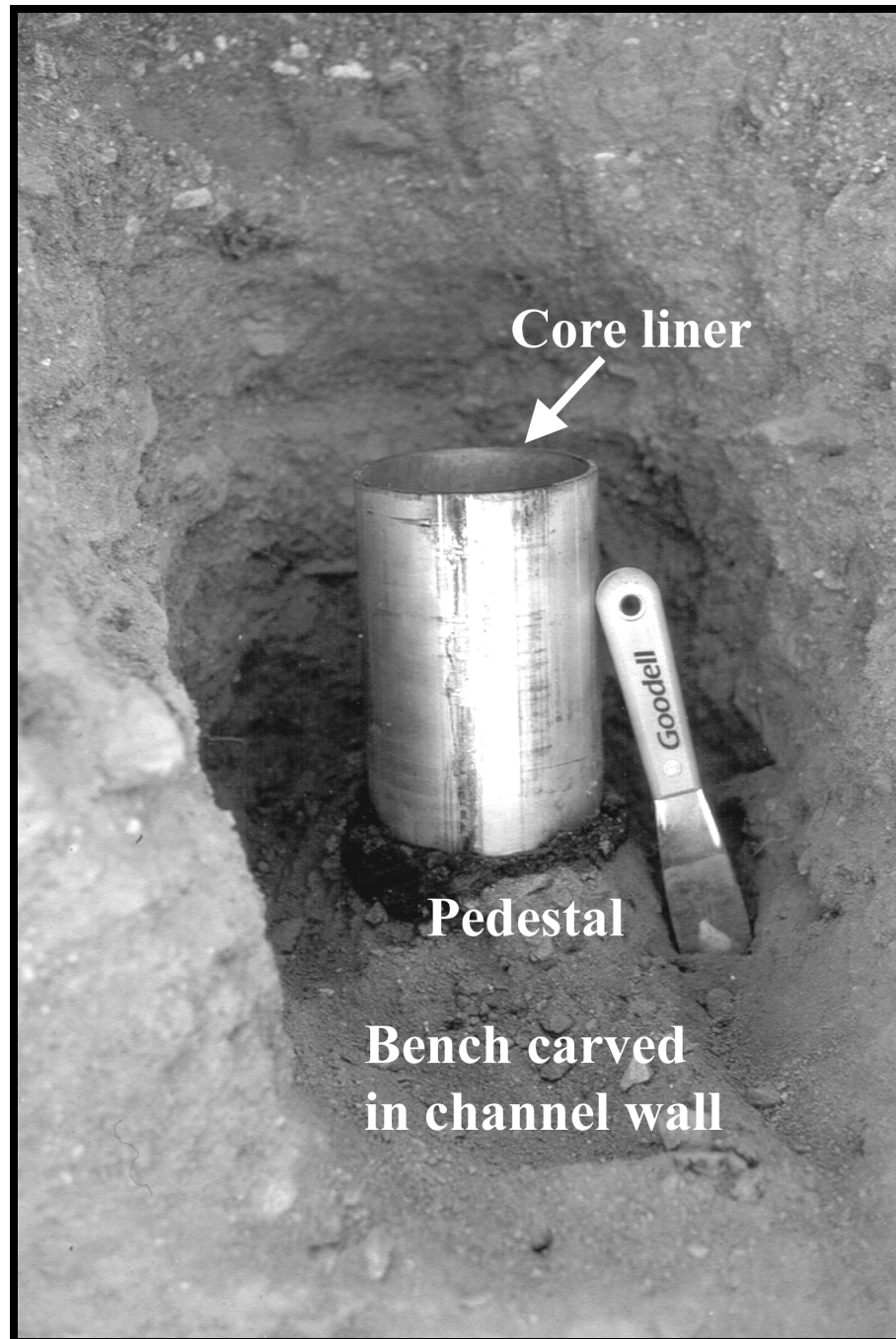


Figure 8. Method of surface core collection along an incised portion of Sheep Creek Wash, July 1998.

Table 1 lists the surface core samples used in this study. Samples were collected along the western channel wall of Sheep Creek Wash near the lower (L) borehole (Fig. 1). All samples were collected at depths of 0.6 to 1.2 m (2 to 4 ft) below the fan surface. At Oro Grande Wash, samples were collected from both the eastern and western channel walls near the lower borehole, L-1 (Fig. 1), at depths of 1.5 to 4 m (5 to 13 ft).

## EXPERIMENTAL METHODS

Water-desorption curves were measured on undisturbed core samples by extracting water in fixed steps, either by forced extraction or by evaporation, and by allowing pressure to equilibrate with time. For the pressure range from 0 to about -500 cm H<sub>2</sub>O, equilibrium  $\psi$  values were measured with a tensiometer-transducer system after extracting water by applying an external suction to the sample (Fig. 9). For pressures less than -500 cm H<sub>2</sub>O, forced evaporation of water was used to control  $\theta$ , with  $\theta$  determined by sample weighing. The filter paper method was used to determine the equilibrium  $\psi$  values. Bulk physical properties, such as particle-size distribution, bulk density, and particle density, were measured after retention measurements were completed and after the core samples were oven-dried.

### Wetting Solution

Five different batches of the wetting solution, a mixture of deionized water, 6 % sodium hypochlorite, NaOCl, and calcium chloride, CaCl<sub>2</sub>·2H<sub>2</sub>O, were used for saturating the samples and for filling the tensiometer and plumbing. Calcium chloride was added to deionized water, in concentrations of 1.5 g/L, to minimize clay dispersion. Three drops of reagent-grade sodium hypochlorite were added per liter of water to inhibit growth of bacteria in the ceramic plate of the tensiometer (Fig. 9) or within the soil pores. The batches, with an average molarity of 0.078  $\mu$ M NaOCl and 9.98  $\mu$ M CaCl<sub>2</sub>·2H<sub>2</sub>O, were closely replicated in order to have uniform liquid conditions for all samples.



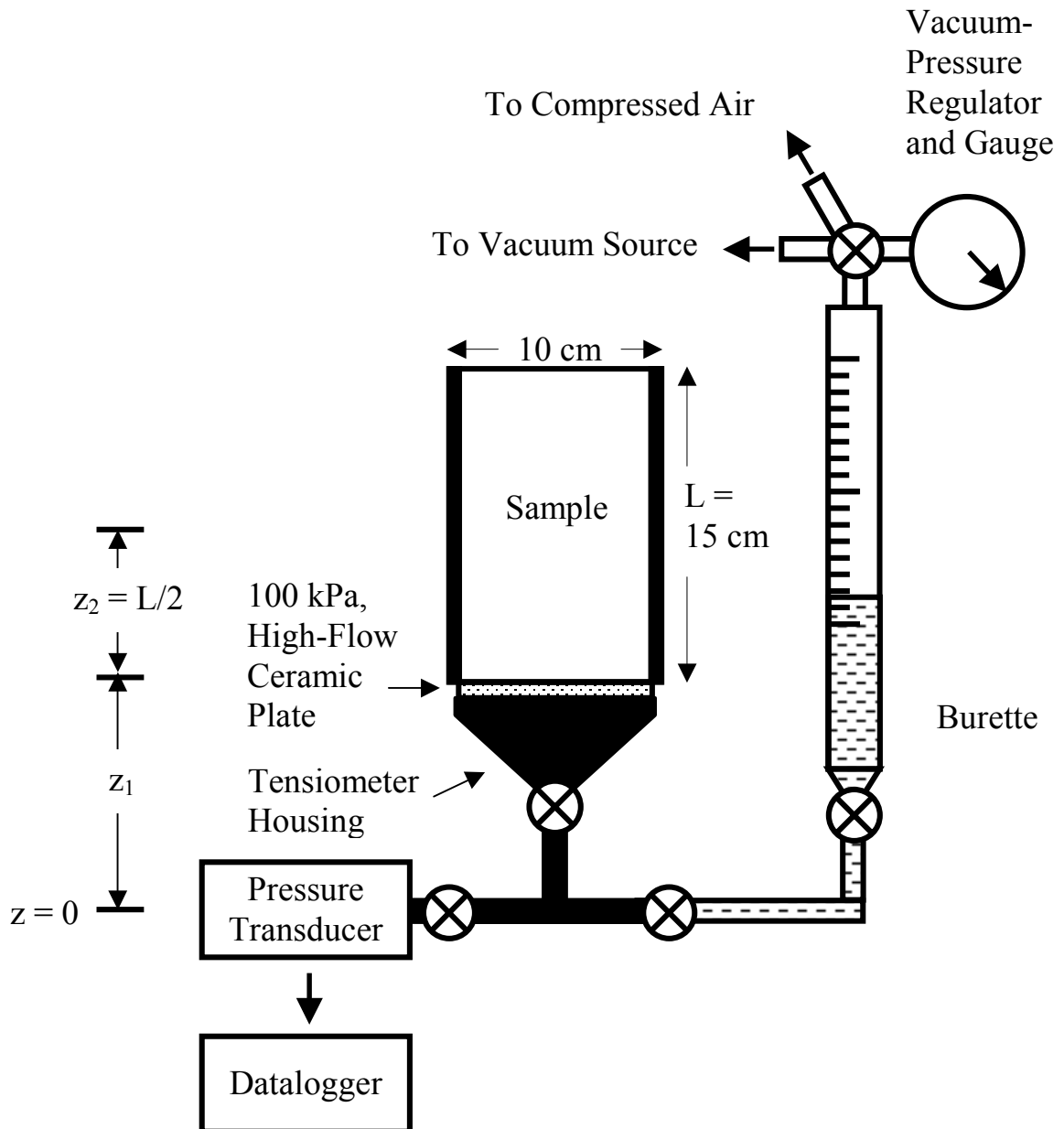


Figure 9. Laboratory apparatus designed to rapidly measure water retention on large core samples (after Su and Brooks, 1980).

Surface tension measurements for each batch were performed using a du Nuoy tensiometer (CSC Scientific Company, model 70535). The average surface tension for all batches was  $0.0748 \pm 0.0002$  N/m at an average temperature of  $22.6 \pm 0.5$  °C.

### Sample Saturation

Each sample in its original core liner was immersed in a dish of the wetting solution, which covered at least half of the sample length, and wetted to apparent saturation. The base of the sample was covered with a screen and perforated cap, allowing water to imbibe from the bottom. The sample was left to sit for a period of a few days, then removed from the dish, and weighed. This was repeated until the change in weight of the sample was less than about 10 g. The final saturated weight,  $W_{\text{sat}}$ , was recorded immediately before the measurement of retention data for later determination of the saturated water content,  $\theta_{\text{sat}} = (W_{\text{sat}} - W_{\text{od}})/\rho_w V_{\text{tot}}$ , where  $W_{\text{od}}$  is the oven-dry sample weight,  $\rho_w$  is the density of water, and  $V_{\text{tot}}$  is the sample bulk volume.

### Water-Retention Curves

#### Controlled Liquid-Volume Method (0 to -500 cm H<sub>2</sub>O)

General. The technique used to measure water retention was modeled after Su and Brooks (1980) where the water content of a sample is controlled and pressure is allowed to equilibrate with time. To determine equilibrium pressures, the technique was modified from a “null method” (Su and Brooks, 1980; Klute, 1986), where the applied pressure is adjusted until it matches that of the soil, to one where pressure is monitored

with time using a pressure transducer. Traditional measurement techniques that utilize a pressure-plate or Tempe cell, where pressure is controlled and water content is allowed to redistribute with time, are more time-consuming and generally work best for small, disturbed samples (Richards, 1941; Klute, 1986). Advantages of the technique used here include rapid measurement of points on the retention curve and the ability to use large, undisturbed cores.

Equipment. The apparatus used for this study (Fig. 9) consisted of a tensiometer (porous ceramic plate attached to a steel housing and pressure transducer), a large (250 ml) burette, a vacuum-pressure regulator, and a datalogger. The tensiometer was custom designed using a high-flow ceramic plate, with a bubbling pressure of -1000 cm H<sub>2</sub>O (100 kPa), fit to a specially designed stainless-steel housing. The housing was connected at its base to stainless-steel plumbing, which was attached both to the transducer and to tubing to the burette. The connection between the burette and the tensiometer consisted of translucent polyethylene tubing, allowing the formation of air bubbles at low (more negative) matric pressure head values to be visually monitored. The transducer was connected to a datalogger to monitor pressure at the base of each sample with time.

Procedure. The transducer was calibrated by recording output voltages for different heights of a hanging water column relative to the center of the transducer, taken as the reference elevation,  $z = 0$  (Fig. 9). Output voltages from the transducer were converted to pressure values according to the calibration formula,  $P = (\Delta P/\Delta V)(V - V_0)$ , where  $\Delta P/\Delta V$  is the slope of the line for at least three measured pressure and voltage pairs and  $V_0$  is the voltage at  $z = 0$ . A datalogger was programmed to calculate pressures using

these calibration data. At the end of each sample run, the equilibrium matric pressure values,  $\psi$ , were adjusted to the midpoints of all samples by subtracting  $z_1$ , the distance between the transducer and the ceramic surface in contact with the sample, and  $z_2$ , half of the measured core length (Fig. 9).

The tensiometer, stainless-steel plumbing, and polyethylene tubing were flushed with the deaerated wetting solution until all trapped air was removed from the system. After saturation, the sample was placed on the tensiometer and both ends were wrapped with plastic to minimize evaporation. To ensure good contact between the ceramic and the base of the sample, the sample was clamped upright between two plastic shelves on a system of steel bars. To measure a volumetric water content,  $\theta$ , the valve at the base of the burette was opened and the external suction was increased gradually using the vacuum-pressure regulator until a fixed volume of water was extracted into the burette. The average  $\theta$  for the sample was later determined by dividing the cumulative volume of water extracted from the sample at each step,  $V'$ , by the bulk volume,  $V_{\text{tot}}$ , and subtracting the resulting value,  $\theta'$ , from the saturated water content,  $\theta_{\text{sat}}$  (Table 2).  $\theta_{\text{sat}}$  is the maximum water content at an essentially zero  $\psi$  value and usually includes some entrapped air. After water was extracted from the sample, valves to the burette were closed, and the matric pressure head within the sample was allowed to equilibrate with time. Equilibrium was established when the pressure recorded by the transducer became constant with time, typically fluctuating by less than -10 cm H<sub>2</sub>O (Fig. 10). The steps involving water extraction and pressure equilibration were repeated to describe points along a drying curve.

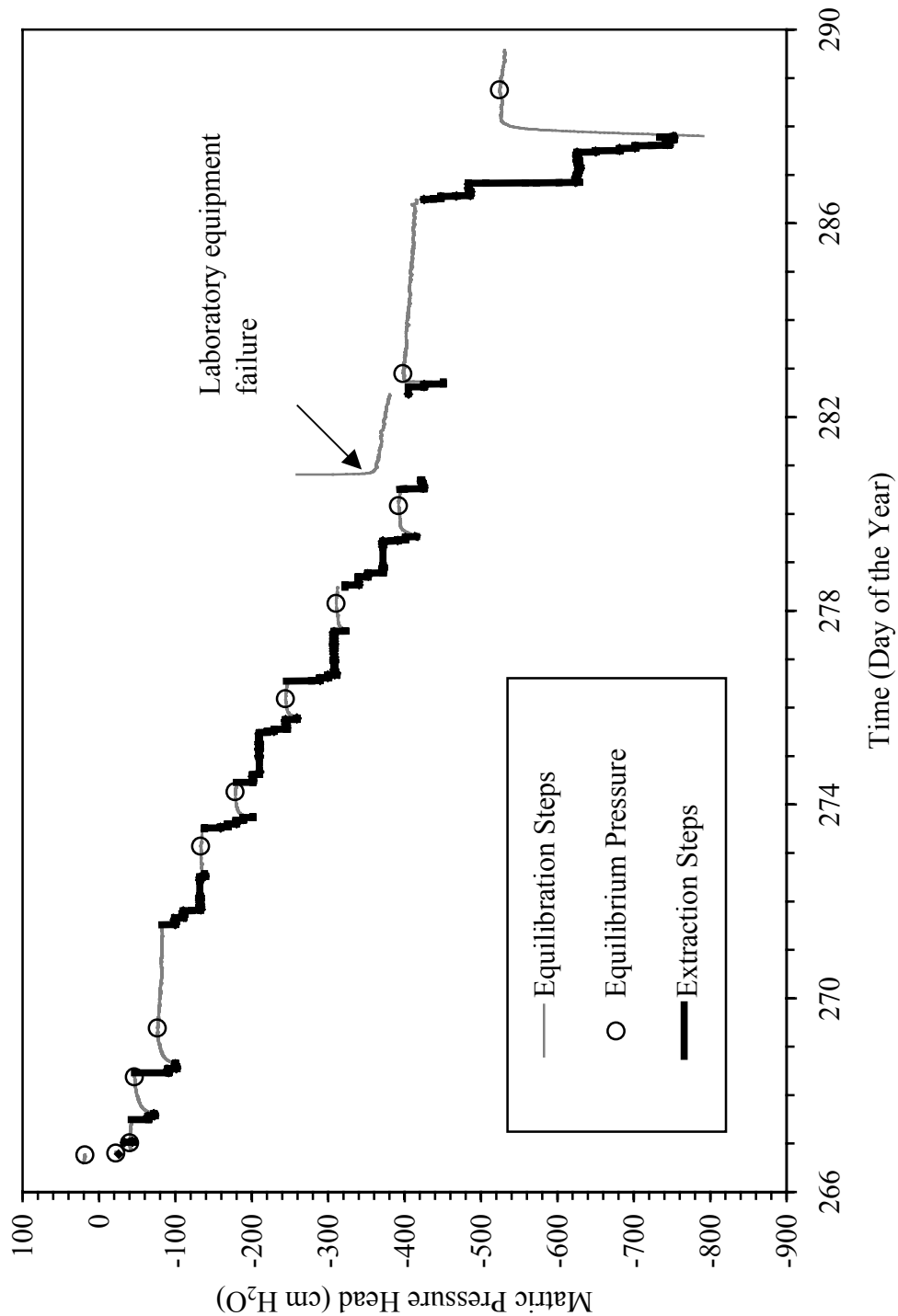


Figure 10. Example output record from the pressure transducer, collected using a datalogger, for sample SCW-1.

Table 2. Example Calculation of Volumetric Water Contents

Bulk Volume of Sample, $V_{tot}$		1000 $\text{cm}^3$
Saturated Water Content, $\theta_{sat} = (W_{sat} - W_{od})/\rho_w V_{tot}$		0.275 $\text{cm}^3/\text{cm}^3$
Cumulative Volume Extracted, $V'$	$\theta' = V'/V_{tot}$	$\theta = \theta_{sat} - \theta'$
ml	$\text{cm}^3/\text{cm}^3$	$\text{cm}^3/\text{cm}^3$
0	0.000	0.275
10	0.010	0.265
30	0.030	0.245
60	0.060	0.215
100	0.100	0.175
250	0.250	0.025

As the sample became drier, the vacuum-regulator pressure was decreased relative to that of the sample pressure in order to drive flow towards the burette. Because the burette remains stationary throughout the experiment, it becomes increasingly difficult to extract water as the water level in the burette rises, therefore the external pressure must be decreased accordingly. When the height of water rises to the maximum capacity of the burette, the burette must be drained. Figure 10 shows a complete pressure record for a sample, including both extraction and equilibration steps, with pressure readings averaged every 5 minutes. Because the transducer records pressure when the valve is open to the burette, the effect of decreasing the external pressure is observed as the extreme negative steps, at lower  $\psi$  values than the equilibrium pressure values.

Because the measurement of water retention is temperature sensitive, laboratory temperature was also monitored with time using a hygrothermograph (Weathertronics, model 5020-A). In cases where the laboratory temperature control failed and fluctuations in the pressure record occurred due to diurnal temperature changes, the equilibrium

pressure was taken as the average value between pressures occurring at the maximum and minimum temperatures.

#### Filter Paper Method and Forced Evaporation of Water ( $< -500$ cm H<sub>2</sub>O)

General. Retention points beyond the range of the controlled-volume apparatus (typically  $< -500$  cm H<sub>2</sub>O) were obtained using the filter paper method for  $\psi$  (Hamblin, 1981; Campbell and Gee, 1986; Greacen and others, 1987). Water contents were controlled by forcing water to evaporate from the sample surface using a fan. The filter paper method is relatively fast, easy to apply, and involves very minimal sample disturbance. A filter paper is placed in contact with the sample, and moisture is transferred to the filter paper until an equilibrium pressure is reached between the sample and the filter paper. This pressure is determined by measuring the water content of the filter paper and from the known retention curve of the filter paper. Forcing water to evaporate from the samples speeds up the collection of data points.  $\theta$  can be determined by directly weighing the samples after equilibration with the filter paper.

Procedure. Because no standard procedure exists for this method, a procedure was followed according to best judgment. To determine different  $\theta$  points, the volume of water was controlled by forcing evaporation from the samples using a fan to increase air flow. The amount of water evaporated was chosen to correspond roughly to amounts extracted using the controlled-volume apparatus. The sample was weighed immediately after removal of the filter papers to determine the average volumetric water content,  $\theta = (W - W_{od})/\rho_w V_{tot}$ , of the sample.

Whatman No. 42 filters, 90 mm diameter, were chosen because of the availability of published retention curves for this type of filter paper. Due to the large size of the samples, a filter paper was placed on each end of the sample, to allow averaging of the pressure head between the two ends. A single filter paper was placed in contact with the sediment, followed by foil or plastic, to prevent evaporation, and the original core liner cap. A period of seven days was chosen as a reasonable equilibration period (periods between 1.5 days (Hamblin, 1981) and 7 days (Fawcett and Collis-George, 1967; Chandler and Gutierrez, 1986; Greacen and others, 1987) have been used by previous workers). The filter was then carefully removed from the sample, one end at a time, and immediately weighed using an analytical balance with accuracy to 0.1 mg. Because water from the filter paper immediately begins to evaporate, the filter paper weight was recorded with time. A linear fit to this time series allowed extrapolation to the weight at time zero, representing the moment when contact was broken between filter and sample. The filter was then oven-dried overnight and its weight recorded to determine its gravimetric water content,  $f$ . From the known retention curve,  $f(\psi)$ , of the filter paper (Fawcett and Collis-George, 1967; Greacen and others, 1987),  $f$  was used to calculate the associated pressure. An approximate equilibrium pressure for the entire sample,  $\psi$ , was determined by averaging the pressures calculated for both ends of the sample. Pairing the average water content and equilibrium pressure for the sample yielded a point on the drying curve. In order to compare  $\psi$  values obtained by the controlled-volume method with those of the filter paper method, a point on the retention curve was obtained using



the filter paper method immediately after removing the sample from the controlled-volume apparatus.

### Bulk Properties

#### Core Extraction and Description

After the last filter paper measurement and before oven drying, samples were extracted from their liners, cut in half, and visually examined. Layering, color, and general particle-size trends were noted, as well as any indication of sedimentary structure arising from depositional environment. For example, any evidence of grading of particle sizes along the length of the sample or of gravel clasts embedded in a finer matrix was noted.

#### Oven-Dryness

After all water-retention points were obtained, the sample was removed from its liner and oven-dried at 105 °C. Samples were weighed several times out of the oven over the course of a few weeks to ensure that the change in weight was  $\leq 1$  g.

#### Porosity

Bulk density,  $\rho_{\text{bulk}}$ , was determined by dividing the oven-dry weight,  $W_{\text{od}}$ , of the sample by the bulk volume,  $V_{\text{tot}}$ . Bulk volumes were calculated from the dimensions of the cylindrical core liner, with adjustments made to the core length for the presence of any recesses or protrusions at either sample end. Recesses were estimated by taking an

average of several measurements over the sample surface with a depth micrometer.

Protrusion estimates were obtained by measuring the height of material rising above the end of the core liner, at locations around the core circumference only. The particle density for each sample,  $\rho_{\text{particle}}$ , was measured by the pycnometer method, after Blake and Hartge (1986), using about 5 g of randomly scooped, oven-dried subsamples in the size range  $< 0.85$  mm. Porosity was then calculated from the relation

$\Phi = 1 - (\rho_{\text{bulk}}/\rho_{\text{particle}})$ , where the ratio  $\rho_{\text{bulk}}/\rho_{\text{particle}}$  represents the fraction of the bulk volume occupied by solids.

#### Particle Size

After oven-drying the samples, particle-size distributions were determined using ASTM sieves (sizes 31.5, 22.4, 16, 11.2, 8, 5.6, 4, 2.8, 2, 1.4, 1, and 0.85 mm) for particle sizes  $> 0.85$  mm and a laser particle-size analyzer (Coulter LS 230 Series) for particle sizes from 0.85 mm to  $4 \times 10^{-5}$  mm. Sieving was performed in two or more steps depending on the amount of sediment. A set of six sieves (31.5 to 5.6 mm or 4 to 0.85 mm) was shaken for a period of 10-15 minutes using a Ro-Tap machine. For a few samples with coarse fractions  $> 31.5$  mm, ASTM sieves (sizes 90, 63, and 45 mm) were used to refine this end of the particle-size distribution. Sediment was carefully removed from the screens by tapping or by using sieve brushes. The fraction of sediment  $< 0.85$  mm was then split into subsamples using a spinning riffler because the optical analyzer requires small sample sizes. Subsamples on the order of 0.5-1 g were used depending on texture. The optical analyzer uses the Fraunhofer diffraction model to calculate particle

sizes (assumed spherical) based on optical diffraction of a laser beam passed through a slurry of the particles. Samples were loaded into a fluid module containing filtered tap water. Sonication during loading of the sample was used to disperse aggregates. Because the optical analyzer computes sizes on a 100% volume scale relative to the sample mass fraction  $< 0.85$  mm, optical data were renormalized from a volume basis to a mass basis and integrated with the sieve data. This placed both methods of analysis on a mass basis relative to the total sample weight, so that all size fractions summed to 100 %. The particle density was assumed to be uniform between the coarse, or sieve, fraction and the optically analyzed, fine fraction.

In order to compare particle-size distributions to pore-size distributions, particle diameters, from sieve openings and optical channels, were converted to radii. Because the  $\Delta r$  intervals between sieve and optical data are not equal, points were added between the sieve data by geometric interpolation, creating new bins with  $\Delta r$  intervals as close as possible to those of the optical data. On a logarithmic scale, the  $\Delta r$  interval is defined as  $\log(r_{\text{upper}}) - \log(r_{\text{lower}})$ , or  $\log(r_{\text{upper}}/r_{\text{lower}})$ , where  $r_{\text{upper}}$  represents the upper bin limit and  $r_{\text{lower}}$  represents the lower bin limit. For the optical size range, the average  $\Delta r$  interval was  $\log(r_{\text{upper}}/r_{\text{lower}}) = 0.041$ . For the range of particle sizes determined by sieve analysis, the average  $\Delta r$  interval became  $\log(r_{\text{upper}}/r_{\text{lower}}) = 0.037$  after interpolation.

## METHODS OF DATA ANALYSIS

### Water-Retention Data

#### Empirical Curve Fits to Measured Data

After obtaining points on the drying curve for each sample, an empirical curve was fitted to the data using the form developed by van Genuchten (1980) and the regression analysis program RETC (van Genuchten and others, 1991). The empirical formula has the form:

$$\theta(\psi) = \theta_r + \{(\theta_{\text{sat}} - \theta_r) / [1 + (\alpha\psi)^n]^m\}$$

where:  $\theta_r$  = residual water content

$\theta_{\text{sat}}$  = saturated water content

$\alpha$ ,  $n$ , and  $m$  = empirical fit parameters

The program fits  $\theta$  against measured  $\psi$  values, and optimizes the empirical parameters  $\alpha$  and  $n$ .  $\theta_{\text{sat}}$  is typically a known input for fitting the curve, whereas  $\theta_r$  is chosen to be a fixed or an optimized value. The empirical parameter  $m$  was set equal to  $1 - 1/n$  (after van Genuchten, 1980). This restriction reduces the number of independent parameters in the model, allowing better model convergence, and is imposed when data cover a limited range of  $\psi$  or show much scatter (van Genuchten and others, 1991). Least squares residuals, or goodness of fit values, are also calculated by the RETC code.

Because pore-size distributions are calculated from the van Genuchten curves, it was necessary that the curves represent the available pore space for drainage and

accurately fit the measured data points. The value of saturation determines the starting point from which desaturation occurs. However if the saturation values are not comparable between samples, then the samples cannot be compared directly. Also, if the values of saturation deviate from porosity by a significant amount, including a lot of entrapped air, which may be an artifact of the saturation technique, then the largest pores will not be represented by the retention curves according to capillary theory. The largest pores are important in distinguishing structural effects due to grain arrangement as shown in Figure 3. Because porosity is an independently determined factor and is chosen as a fixed endpoint during the curve fitting process, porosity was used in place of the measured  $\theta_{\text{sat}}$  values to best represent the largest pore sizes for each sample.

The value of  $\theta_r$  was optimized by the RETC code in order to produce better fits to the measured data points than is possible by setting  $\theta_r$  to a fixed value such as zero or some other appropriate value based on the sample texture. In this study,  $\theta_r$  was determined by setting it as an independent parameter in the program RETC. The program then calculates the best value of  $\theta_r$ , using its nonlinear least-squares regression algorithm, from the measured data points and values of the other independent parameters,  $\alpha$  and  $n$ . A disadvantage to the optimization of  $\theta_r$  based on the measured data points is that it is highly dependent on the measured range of  $\theta(\psi)$  values, especially those points with the lowest water contents.

### Calculation of Pore-Size Distributions

Interpreted according to capillary theory, the water-retention curve of a sample is a measure of its pore-size distribution. When the  $\theta(\psi)$  curve for a drying cycle is translated into a pore-size distribution,  $\theta(r)$ , using differential volume percentages (volume of water drained between pressure points) and capillary theory, this is referred to as the water-desorption technique (Danielson and Sutherland, 1986) for determining pore-size distributions. Pressure values associated with pores draining or filling are converted to effective radii by assuming that capillary tubes can approximate pore shapes. Other methods, such as mercury intrusion and nitrogen adsorption, involve separate measurement of pore-size distribution apart from water-retention measurement. Because sample preservation was required after  $\theta(\psi)$  measurement, for particle-size analysis, oven-dryness, and visual examination of structure, a destructive means of measuring pore sizes, such as impregnating the cores with a resin or intruding the pores with mercury, was not desired. Pore-size distributions calculated using the water-desorption method are more applicable to hydrologic studies than those based on mercury or nitrogen (Nagpal and others, 1972; Lawrence, 1977; Ragab and others, 1982; Danielson and Sutherland, 1986). Common sources of inaccuracy with the water-desorption method include air-entrapment (depending on the state of saturation and pathway of water drainage), change in structure (common in clay soils that shrink or swell), and the idealization of pores as capillary tubes.

Normally, to calculate a cumulative pore-size distribution using the water-desorption technique,  $\theta$  and  $\psi$  pairs are determined by measuring a drainage curve and

each  $\psi$  value is converted to an effective pore size using capillary theory. Because the measured  $\psi$  values varied for each sample in this study as a result of the measurement technique (controlling  $\theta$  and letting  $\psi$  equilibrate with time), the van Genuchten function was used to determine  $\theta(\psi)$  from the unique fit parameters for each sample, with the  $\psi$  values based on predefined values of pore radii chosen to correspond exactly to the radii utilized for particle-size measurements. From the relationship  $\theta(r)$ , water contents were then normalized according to the formula for percent saturation,  $S = (\theta - \theta_r)/(\Phi - \theta_r)$ , where  $\Phi$  is the porosity and  $\theta_r$  is the residual water content. Each  $S$  value was then paired with the pore radius corresponding to each water content value to define a cumulative pore-size distribution,  $S(r)$ , on a 100 % basis. Because the range of pore sizes is finer than the range of particle sizes, size intervals were added at the fine end of the pore-size distributions, using the average logarithmic optical  $\Delta r$  interval of 0.041, to produce cumulative frequency distributions that started from zero percent and histograms that summed to 100 %.

Cumulative pore-size distributions were used to calculate pore-size statistics (Folk, 1980) and pore-size histograms (Danielson and Sutherland, 1986). From the  $S(r)$  curve, pore-size histograms were created by subtracting the volume percentages between adjacent pore radii. Then each volume percentage was assigned to the arithmetic center of the corresponding  $\Delta r$  interval. Because the shapes of the pore-size histograms are influenced by bin size, all differential pore-size distributions were calculated using the same values of pore radii, corresponding exactly to the sieve and optical particle-size

radii. This enabled pore-size histograms to be compared directly between samples and with the measured particle-size histograms.

### Textural Classification

After measuring the particle-size distributions for each sample, textural classes were defined in terms of percentages of gravel, sand, silt, and clay using the Wentworth (1922) size classification. After the method of Folk (1980), textural classes were then used to assign a textural name to each sample. For example, a sample with a texture of gravelly sand, gS, has a ratio of sand to mud (silt plus clay) of at least 9:1 and gravel content between 5 and 30 %.

### Graphical Statistics

From the cumulative frequency distributions for both particle size and pore size, graphical statistics, including the mean, median, inclusive graphic standard deviation (sorting), inclusive graphic skewness, and kurtosis, were calculated from the formulas defined by Folk (1980). Because these formulas were created for use with percent-coarser-than cumulative distributions, some of the percentiles in the formulas for the inclusive graphic sorting, inclusive graphic skewness, and kurtosis were changed to accommodate the percent-finer-than cumulative distributions used in this study. For example, the radius at the 84<sup>th</sup> percentile on a percent-coarser-than distribution corresponds to the radius at the 16<sup>th</sup> percentile on a percent-finer-than distribution, and so on. Pore and particle sizes in mm were determined at  $r_5$ ,  $r_{10}$ ,  $r_{16}$ ,  $r_{25}$ ,  $r_{50}$ ,  $r_{60}$ ,  $r_{75}$ ,  $r_{84}$ , and



$r_{95}$ , where the subscript denotes the percentage finer than the given radius. These radii were converted to  $\phi$  values, where  $\phi = -\log_2(r)$ , because the statistical formulas require  $\phi$  units. After statistical calculations, the mean and median pore and particle sizes were converted from  $\phi$  units back into mm, and sorting was kept in  $\phi$  units. The other statistical parameters are dimensionless. The uniformity coefficient,  $C_u = r_{60}/r_{10}$ , was calculated as an alternative measure of sorting.

## RESULTS

### Bulk Properties

The bulk property measurements for all cores, including bulk density, particle density, and porosity, are listed in Table 3. The average particle density for samples from Oro Grande Wash is 2.71 g/cm<sup>3</sup> and the average value for Sheep Creek Wash is 2.75 g/cm<sup>3</sup>, although individually measured values are used in calculations of porosity. For each sample, the measured saturated water content,  $\theta_{\text{sat}}$ , and the percent saturation relative to porosity,  $\theta_{\text{sat}}/\Phi$ , are included.

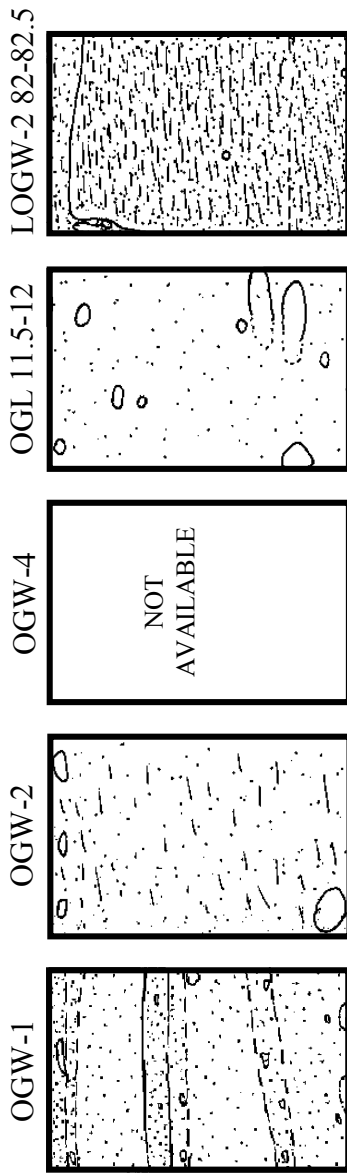
Table 3. Bulk Properties

Sample	Depth		$\rho_{\text{bulk}}$	$\rho_{\text{particle}}$	Porosity, $\Phi$	$\theta_{\text{sat}}$	% Saturation ( $\theta_{\text{sat}}/\Phi$ )
	m	ft	g/cm <sup>3</sup>	g/cm <sup>3</sup>		cm <sup>3</sup> /cm <sup>3</sup>	
OGW-1	~1.5	~5	1.73	2.79	0.379	0.244	64.2
OGW-2	~2.4	~8	1.70	2.66	0.359	0.278	77.4
OGW-4	~4	~13	1.79	2.65	0.323	0.299	92.4
OGL 11.5-12	3.5	11.5	1.92	2.69	0.287	0.184	64.1
LOGW-2 82-82.5	25	82	1.83	2.79	0.343	0.282	82.2
SCW-1	~0.9	~3	1.88	2.77	0.321	0.281	87.6
SCW-2	~0.6	~2	1.67	2.77	0.397	0.299	75.4
SCW-4	~0.6	~2	1.80	2.76	0.350	0.280	80.0
SCF 57-57.5	17.4	57	1.60	2.74	0.417	0.396	94.8
LSCW 58-58.5	17.7	58	1.93	2.71	0.288	0.280	97.6

### Core Description

Core diagrams were created based on observations made from a cross-section along the length of each core (Fig. 11). The cores were described immediately after the last water-retention measurements and before oven drying. Layering and general textural trends were readily identified, although sorting within layers was not discernable.

### ORO GRANDE WASH SAMPLES



### SHEEP CREEK WASH SAMPLES

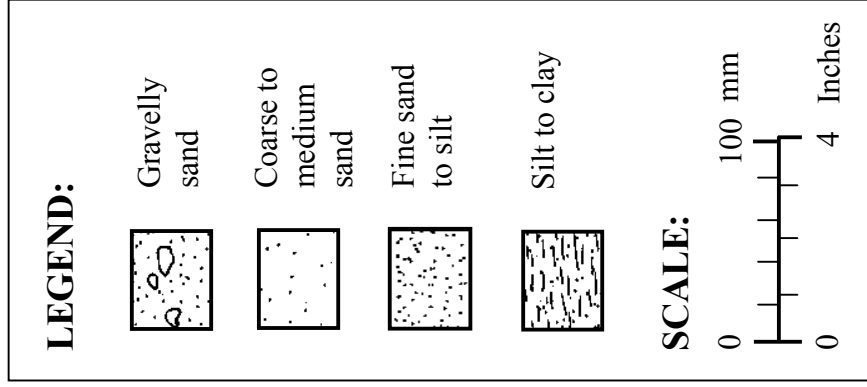
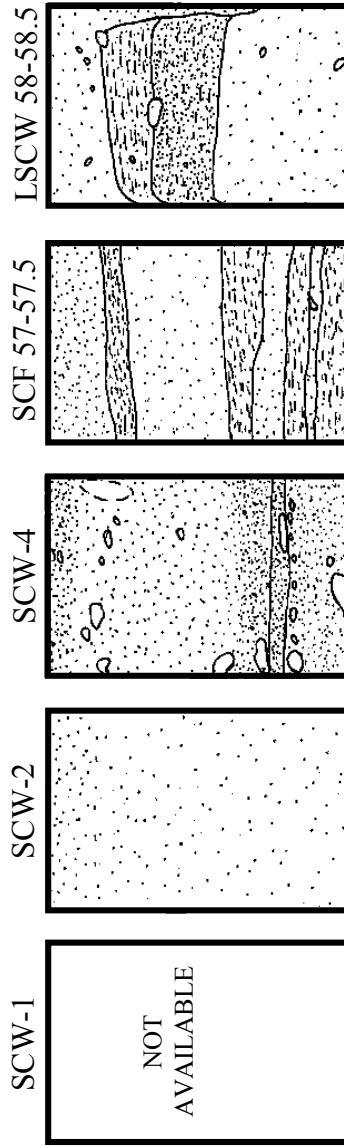


Figure 11. Sketches of core structure for Oro Grande Wash and Sheep Creek Wash samples after the completion of water-retention measurements.

### Particle-Size Distributions and Statistics

Textural class percentages determined from the measured particle-size distributions, as well as the textural class nomenclature for each sample, are presented in Table 4. The cumulative frequency distributions for Oro Grande Wash and Sheep Creek Wash samples are shown in Figure 12. The distributions are summations starting from the smallest detectable particle radius of  $2 \times 10^{-5}$  mm and are plotted as the percentage of particles finer than a given radius. Particle-size histograms, plotted as the weight percent of particles corresponding to the arithmetic mean of each  $\Delta r$  interval, are shown in Figure 13 for each wash.

Table 4. Textural Classification

Sample	Textural Class	% Gravel	% Sand	% Silt	% Clay
		(> 2 mm)	(2-0.06 mm)	(0.06-0.004 mm)	(< 0.004 mm)
OGW-1	gS, gravelly sand	18.11	79.01	2.13	0.69
OGW-2	gS, gravelly sand	21.38	74.99	2.76	0.85
OGW-4	gzS, gravelly silty sand	12.65	69.56	15.25	2.59
OGL 11.5-12	zsG, silty sandy gravel	50.31	44.58	4.09	1.35
LOGW-2 82-82.5	gzS, gravelly silty sand	8.35	62.52	26.52	2.96
SCW-1	gzS, gravelly silty sand	11.98	67.31	17.61	3.19
SCW-2	gS, gravelly sand	9.01	84.29	5.41	1.28
SCW-4	gzS, gravelly silty sand	24.80	64.79	8.69	1.68
SCF 57-57.5	(g)zS, slightly gravelly silty sand	2.32	52.33	37.90	7.64
LSCW 58-58.5	gzS, gravelly silty sand	8.68	53.91	30.07	7.56

From the cumulative frequency distributions, graphical statistics, including mean and median particle radius, sorting, kurtosis, and skewness, were calculated after Folk

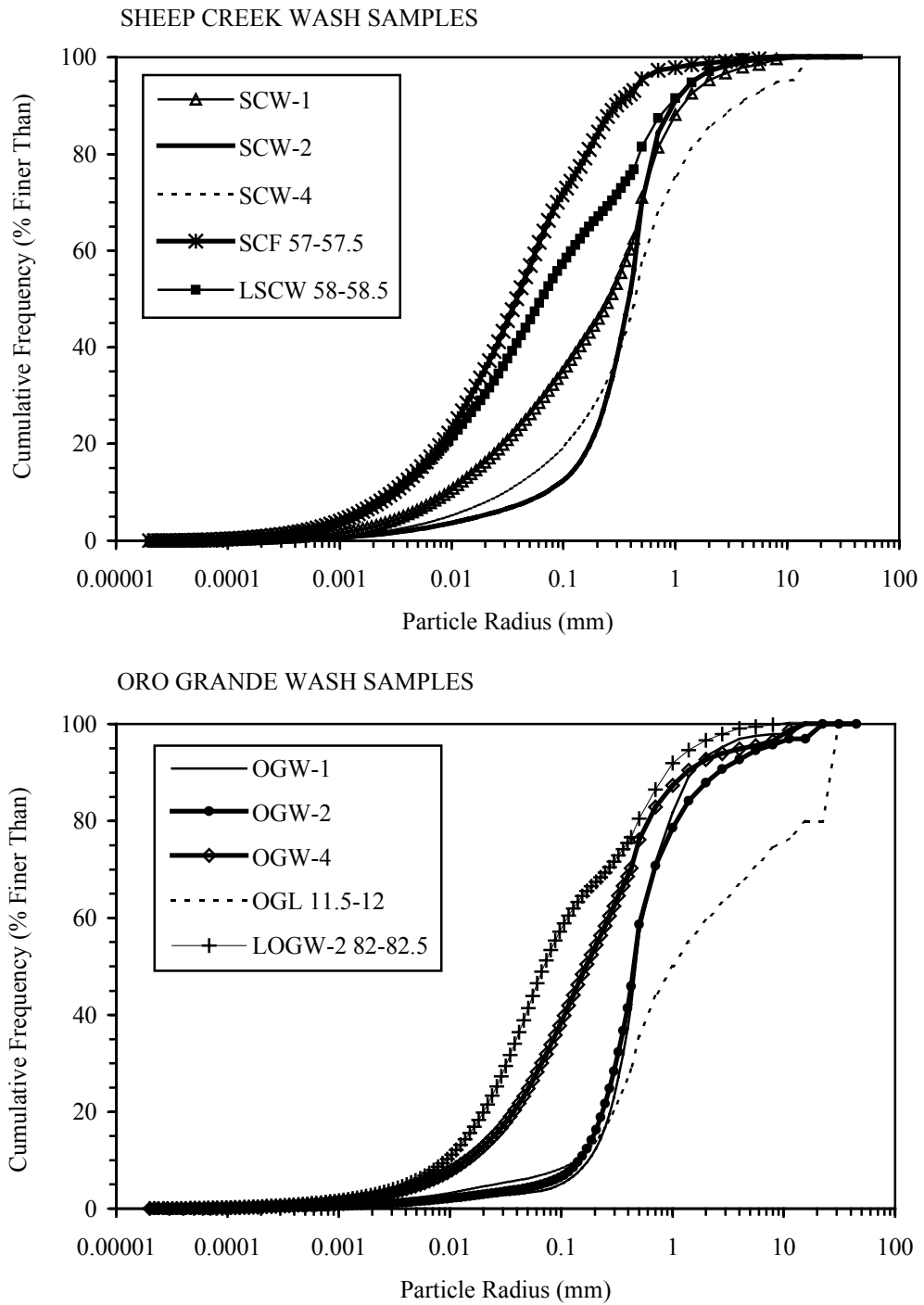


Figure 12. Particle-size distributions, plotted as cumulative percentage by weight finer than a given size fraction, for samples from Sheep Creek Wash and Oro Grande Wash.

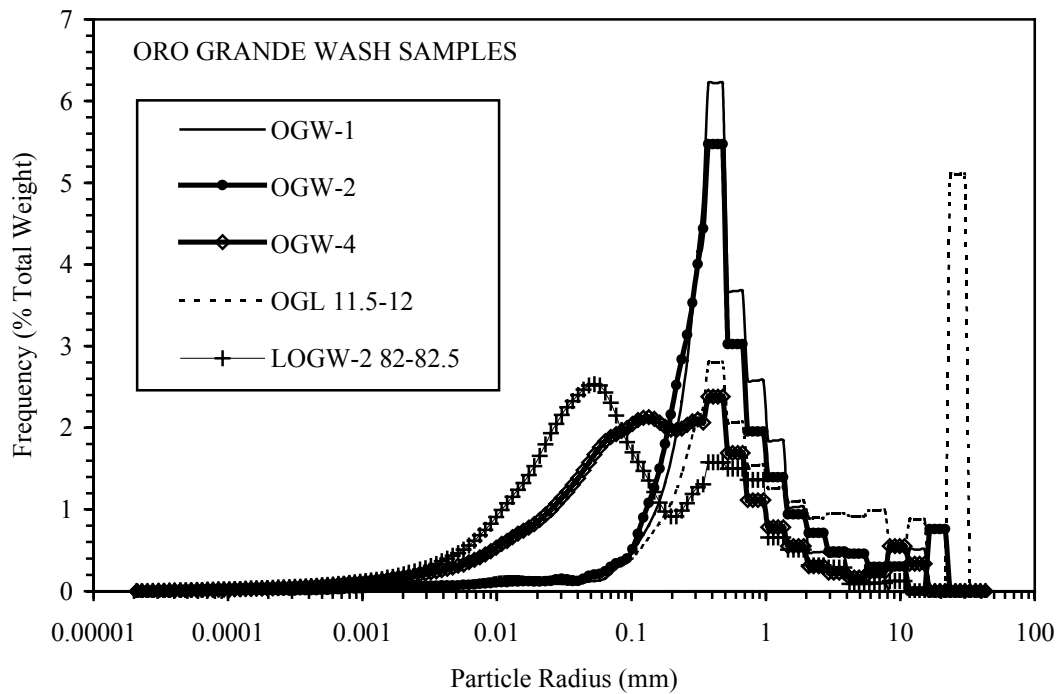
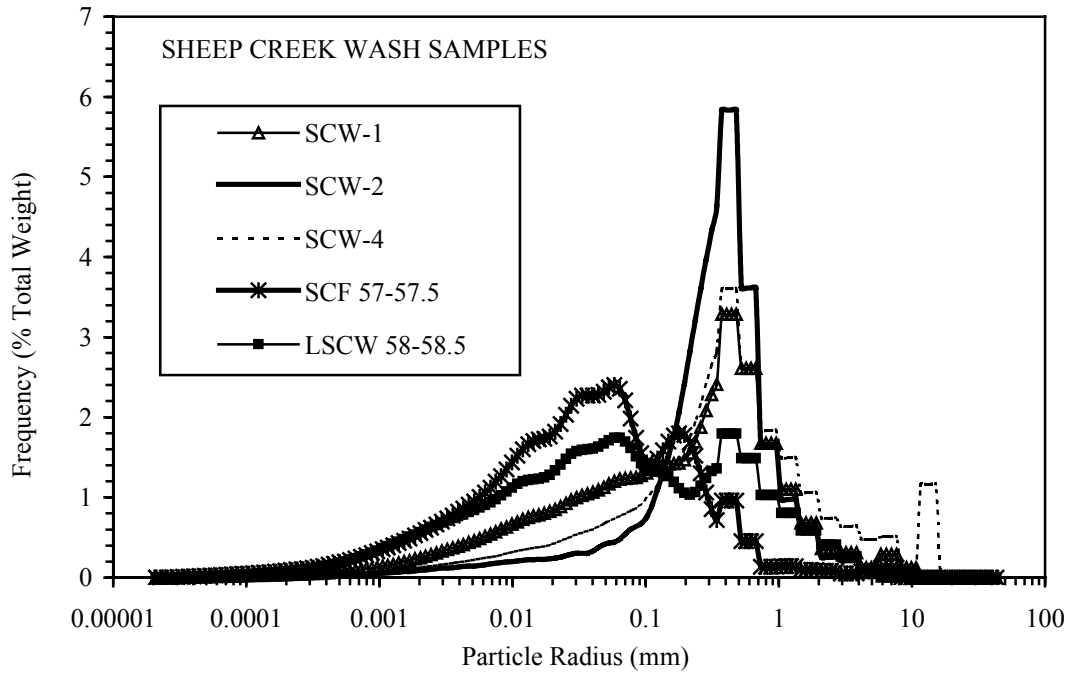


Figure 13. Particle-size histograms, plotted as frequency percent by weight, for samples from Sheep Creek Wash and Oro Grande Wash.

(1980). The uniformity coefficient,  $C_u = r_{60}/r_{10}$ , was calculated as an alternate measure of sorting (Table 5). Sorting values less than 1  $\phi$  unit indicate a narrow size distribution (well-sorted materials) with progressive widening of the size distribution (poorly sorted materials) for values larger than 1  $\phi$ .

Table 5. Particle-Size Statistics

Sample	Mean Radius	Median Radius	Sorting	$C_u$	Skewness	Kurtosis
	mm	mm	$\phi$		$\phi/\phi$	$\phi/\phi$
OGW-1	0.4919	0.4500	1.28	3.1	-0.12	1.42
OGW-2	0.4865	0.4330	1.67	3.8	-0.18	1.59
OGW-4	0.1446	0.1550	2.66	18.9	0.03	1.22
OGL 11.5-12	1.7366	0.9900	3.18	16.3	-0.16	0.89
LOGW-2 82-82.5	0.0834	0.0690	2.63	12.8	-0.09	0.88
SCW-1	0.1547	0.2500	2.72	41.3	0.37	1.03
SCW-2	0.3229	0.3700	1.55	6.3	0.32	1.88
SCW-4	0.3676	0.4300	2.62	18.4	0.13	1.48
SCF 57-57.5	0.0348	0.0370	2.57	18.7	0.09	1.01
LSCW 58-58.5	0.0601	0.0625	3.15	40.0	0.07	0.85

### Water-Retention Properties

Measured retention points obtained by desaturating the samples from apparent saturation are shown in Figure 14. The van Genuchten (1980) formula was used to fit a curve to the data points. Due to significant amounts of trapped air for some samples,  $\theta_{sat}$  values deviate from porosity,  $\Phi$ , by as much as 40 % (Table 3). To represent the larger pore sizes and produce better fits to the measured points, porosity was used in place of  $\theta_{sat}$  for the determination of van Genuchten parameters. Using porosity improved the fit to the measured retention points near the air-entry pressure, with the exception of sample LOGW-2 82-82.5. Values of residual water content,  $\theta_r$ , were optimized during the curve

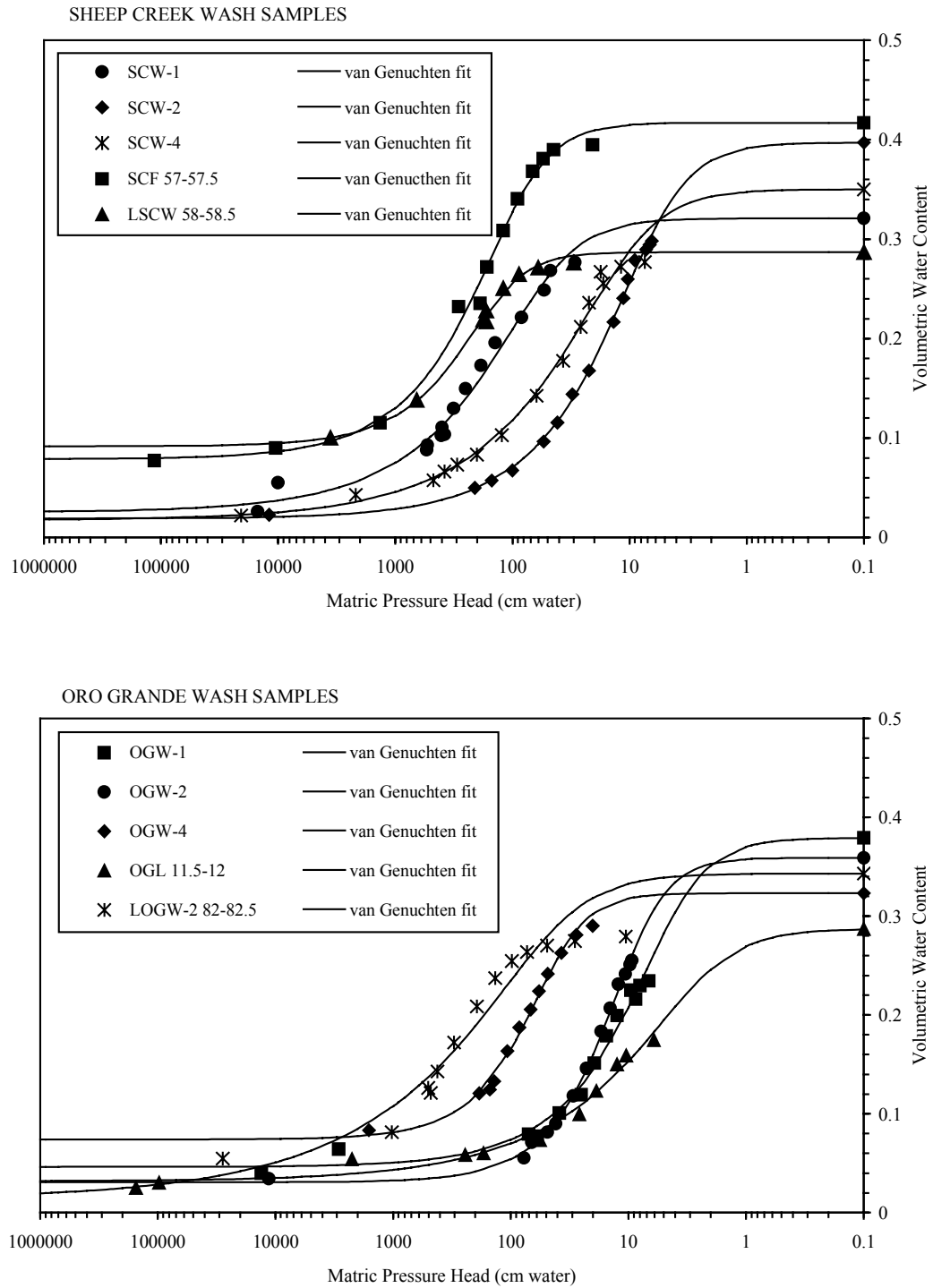


Figure 14. Water-retention measurements and curves fitted using the empirical function of van Genuchten (1980) for Sheep Creek Wash and Oro Grande Wash.



fit procedure and rely heavily upon the driest measured range of  $\theta(\psi)$ . Because the driest points do not necessarily represent a cessation of drainage from the sample,  $\theta_r$  was used to produce better fits to the measured points rather than to represent physical reality. For each sample, the van Genuchten fit parameters,  $\alpha$ ,  $n$ ,  $m$ , and  $\theta_r$ , and the  $R^2$  coefficient are listed in Table 6. The reciprocal of  $\alpha$  is sometimes referred to as the air-entry pressure of the sample,  $\psi_{ae}$ .

Table 6. van Genuchten Parameters with Calculated  $\Phi$  and Optimized  $\theta_r$

Sample	$\alpha$	$1/\alpha$	n	m	$\theta_r$	$R^2$
	$\text{cm}^{-1}$	cm			$\text{cm}^3/\text{cm}^3$	
OGW-1	0.2165	4.6	1.8095	0.4474	0.0463	0.9873
OGW-2	0.1056	9.5	2.1190	0.5281	0.0307	0.9984
OGW-4	0.0223	44.8	2.1399	0.5327	0.0740	0.9943
OGL 11.5-12	0.3863	2.6	1.5195	0.3419	0.0317	0.9899
LOGW-2 82-82.5	0.0218	45.9	1.4061	0.2888	0.0139	0.9412
SCW-1	0.0173	57.8	1.6241	0.3843	0.0255	0.9871
SCW-2	0.1492	6.7	1.7335	0.4231	0.0191	0.9983
SCW-4	0.0848	11.8	1.5545	0.3567	0.0175	0.9901
SCF 57-57.5	0.0099	101.3	1.8215	0.4510	0.0789	0.9935
LSCW 58-58.5	0.0065	154.6	1.9863	0.4966	0.0917	0.9956

### Pore-Size Distributions and Statistics

Figure 15 represents the pore-size histograms, calculated using the van Genuchten (1980) function and the capillary equation, for each sample. Pore radii were chosen to correspond to the arithmetic center of each particle-size  $\Delta r$  interval. For all samples, surface tension,  $\sigma$ , was taken as the average measured value of all wetting solutions, 0.0748 N/m, the density of water,  $\rho_w$ , was assumed to be 1000  $\text{kg}/\text{m}^3$ , and the contact angle,  $\delta$ , was assumed to equal zero. Graphical statistics (Folk, 1980) were used to

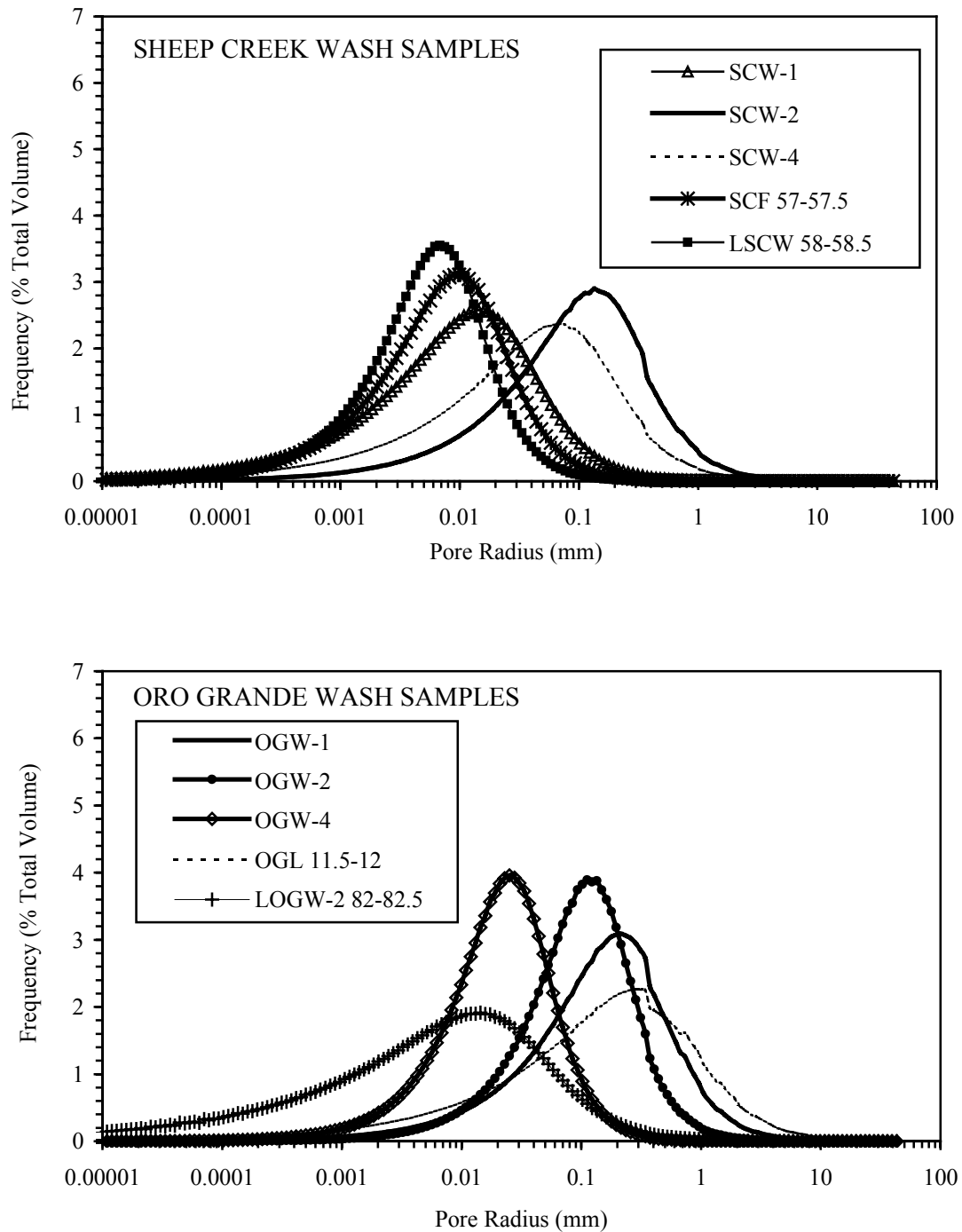


Figure 15. Pore-size histograms, plotted as frequency percent by volume, for samples from Sheep Creek Wash and Oro Grande Wash. Curves are calculated from fits to measured data (Fig. 14) using the van Genuchten (1980) function for retention and capillary theory.

determine the mean and median pore radius, sorting, skewness, and kurtosis. The uniformity coefficient,  $C_u$ , was also calculated (Table 7).

Table 7. Pore-Size Statistics for Curve Fits Using Calculated  $\Phi$  and Optimized  $\theta_r$

Sample	Mean Radius	Median Radius	Sorting	$C_u$	Skewness	Kurtosis
	mm	mm	$\phi$		$\phi/\phi$	$\phi/\phi$
OGW-1	0.1382	0.1600	2.04	11.3	0.20	1.15
OGW-2	0.0886	0.0950	1.57	0.6	0.12	1.17
OGW-4	0.0194	0.0205	1.55	6.0	0.12	1.14
OGL 11.5-12	0.1300	0.1700	2.90	37.1	0.26	1.14
LOGW-2 82-82.5	0.0044	0.0062	3.56	89.7	0.28	1.18
SCW-1	0.0078	0.0097	2.51	20.8	0.24	1.14
SCW-2	0.0826	0.0950	2.19	13.9	0.18	1.15
SCW-4	0.0317	0.0400	2.73	29.8	0.24	1.16
SCF 57-57.5	0.0063	0.0072	1.99	12.5	0.18	1.12
LSCW 58-58.5	0.0050	0.0056	1.73	7.4	0.17	1.08

## ERROR ANALYSIS

### Experimental Errors

#### Matric Pressure Head Errors

For the controlled-volume apparatus, uncertainties in matric pressure head occur during transducer calibration, as a result of laboratory temperature fluctuations, and by determination of the equilibrium pressure head value. Based on the transducer calibration data, the difference between the pressure observed using a hanging water column connected to the transducer and the pressure calculated from calibration values was on the order of 1 to 2 cm. When laboratory thermostat failure occurred, temperature fluctuated by 4 °C for the worst case, but more typically varied on the order of 2 °C or less, causing pressure to vary by  $< 10 \text{ cm H}_2\text{O}$ . Because pressure was monitored at a single point within the sample, at its base, equilibrium could only be determined by observing the pressure time series until deviations became small (on the order of a few  $\text{cm H}_2\text{O}$ ). Uncertainties in  $\psi$  caused by not allowing sufficient time for equilibrium to be reached are likely to be much less than  $10 \text{ cm H}_2\text{O}$ .

With the controlled-volume technique, hysteresis may affect the equilibrium  $\psi$  values. During extraction of water, drainage occurs near the bottom of the sample with subsequent rewetting of this area during pressure equilibration as water redistributes from the upper part of the sample. The resulting  $\psi$  would be displaced slightly away from the true drying curve. The magnitude of this effect on pressure depends on the sample height, the speed of extraction, and the nature of the medium. For a fairly linear

$\psi$  distribution within the sample, the maximum magnitude of error in  $\psi$  is approximated by the sample length or about 15 cm. Hysteresis would produce the largest error at higher equilibrium  $\psi$  values, close to the air-entry pressure. If extraction occurs at a slow enough rate, hysteresis may be insignificant, because water will move uniformly downward through the sample and the ceramic. The degree to which hysteresis affects equilibrium  $\psi$  values using the controlled volume method needs to be further investigated by modeling or additional experimentation.

The filter paper method was used to estimate pressure head values in the dry range of retention, therefore extreme accuracy was not expected. Significant differences in  $\psi$  between the top and bottom of some samples could be due to incomplete equilibration (e.g., as a result of forced evaporation of water), errors during weighing of the filter papers, or compression of the bottom filter paper. The length of time to establish equilibrium was chosen based on values found in the literature, with no means of determining equilibrium besides the actual calculation of pressure using the filter paper and comparing the  $\psi$  values for each sample end. During removal of the filter paper from the sample surface, soil particles often stick to the filter and must be quickly removed to avoid errors in the initial weighing of the filter paper. Because this must be accomplished in a time short enough to avoid changes in the water content,  $f$ , of the filter paper due to evaporation, it is often not possible to completely remove the particles. As a result, these particles must be weighed together with the filter paper throughout the weighing process. For this study, the average weight of particles retained on the filter paper was 0.05 g. If this amount were lost between initial weighing and oven-drying of the filter paper, the

maximum error in  $f$  would be 2 % in the wet range of the filter paper retention curve ( $f > 0.453$ ). The corresponding error in the calculated  $\psi$  value would be 3 %. For the dry range ( $f < 0.453$ ), the maximum error in  $f$  would vary from 2 to 8 %, with the largest error occurring for very small  $f$  values; the resultant maximum error in  $\psi$  from this one error source would be 15 %.

Campbell and Gee (1986) and Greacen and others (1986) discussed additional sources of error concerning the filter paper method. Campbell and Gee (1986) estimated errors in the  $f(\psi)$  relationship to be  $< 10$  % at any given matric pressure head, based on the scatter of measured data points found in the literature. Greacen and others (1986) observed that the  $\psi$  values measured by the filter paper method were always more negative than those measured by either a psychrometer or a tensiometer for the same soil sample. Matric pressure head values measured by the filter paper were about 5 to 10 % lower than the values measured using a tensiometer. Greacen and others (1986) also noted that failure to allow complete equilibration between the filter paper and the soil sample will always yield a matric pressure head value that is more negative than the soil. The reason for the discrepancy between the psychrometer and filter paper measurements may be related to the adsorption of water by the filter paper, which locally decreases the matric pressure head in the soil. At the extreme matric pressure head values (near  $-1 \times 10^5$  cm  $H_2O$ ) measured using a psychrometer, the soil may take longer to equilibrate with the filter paper than the 6 to 7 days allowed.

### Water Content Errors

Errors in measurement of water content can arise during volume extraction using the controlled volume apparatus and in weighing the samples. During volume extraction, the accuracy with which the volume can be measured depends on whether air has entered the tensiometer system. Possible mechanisms of air entry into the tensiometer include diffusion through the polyethylene tubing connecting the burette to the tensiometer, exsolution of gases dissolved in the soil water, failure of the epoxy that bonds the ceramic to the stainless steel housing, or leaks due to faulty plumbing. For a single bubble on the order of  $0.3 \text{ cm}^3$  (ml), as sometimes observed in the polyethylene tubing,  $\theta$  is underestimated by about 0.3 %.

For water contents determined by weighing the samples, the accuracy of the scale, the oven-dry weight, and the bulk volume affect their final values. Uncertainties in the oven-dry weight are less than 1 %, because the samples were weighed more than once over a period of several weeks to verify that the weight fluctuated by  $< 1 \text{ g}$ . Errors in determining water contents by forced evaporation should be small because samples are weighed directly. During the equilibration period of the filter paper with the sample, some water could be lost to evaporation through the sample caps, although this was minimized with the use of foil or plastic. Samples were weighed before and after each equilibration period with a typical net change in  $\theta$  of  $< 1 \%$  (a few grams).

Sample bulk volume is used in all calculations of water content. For all samples, the dimensions of the individual core liners were carefully measured and recorded. Uncertainty arises during measurement of slight recesses or protrusions of the sediment

within the liner. These irregular surfaces must be accounted for by taking several measurements at various locations using a depth micrometer, the average value of which affects the length dimension for the volume of a cylinder. Errors in bulk volume calculation are less than 1-2 %.

Hysteresis errors, as discussed above, are not expected to affect volumetric water contents, which are averages over the entire sample. The effect of hysteresis occurs during pressure equilibration, after volume extraction has stopped.

#### Particle-Size Errors

The measurement of particle sizes was carried out by two methods: sieving and optical analysis. Particle shape, orientation, degree of sieve loading, and time of shaking are factors known to cause errors in the determination of particle sizes by sieve analysis. Because particles must pass through square openings of a given size, the percentage of particles passing through a given sieve opening depends on the orientation of the particles during the sieving process and upon their individual shapes (Gee and Bauder, 1986; Gale and Hoare, 1991). The presence of too much material on a particular sieve can prevent the free passage of particles onto the next smallest screen size, in addition to causing distortion to the screen (McManus, 1988). The amount of time used in shaking the sediment through the nest of sieves also influences the weights obtained for each sieve size (Ingram, 1971; McManus, 1988; Gale and Hoare, 1991). Optical analysis of particle size is also based on the assumption that particles are spherical in shape (Loizeau and others, 1994). However, the presence of elongate particles is more likely to cause



measurement inaccuracies by traditional methods, such as pipette analysis, because platy particles behave as much smaller particles during settling, which produces a greater deviation from Stokes' law (Cooper and others, 1984). Errors in sieve or optical analysis arising from differences in particle shape are difficult to quantify directly, but it should be noted that they exist. Sheep Creek Wash samples have higher percentages of muscovite or schist clasts, which are more elongate or platy in shape than the dominant minerals, quartz and plagioclase, at Oro Grande Wash. As a result, samples from Sheep Creek Wash may be more susceptible to errors in the measurement of particle size than samples from Oro Grande Wash.

### Errors in Data Analysis

#### Empirical Curve Fits

The van Genuchten (1980) formula is an empirical model for retention that is widely used in unsaturated flow models. It was chosen instead of the model by Brooks and Corey (1964) because it appears to yield better fits in general and represents the transition from  $\theta_{\text{sat}}$  to the drainage slope of the water-retention curve, near the air-entry value, more realistically. Errors in the fit parameters affect  $\psi_{\text{ae}}$ , which is calculated directly from the parameter  $\alpha$ , and statistics calculated from the cumulative pore-size distributions.

Because coarse-textured samples were used in this study, a small deviation in  $\psi$  for all points could change the fit parameters significantly, especially when the air-entry value is very high (e.g., between 0 and -10 cm H<sub>2</sub>O). If all retention points were shifted

by 10 cm, this would produce a large change in the higher  $\psi$  values (those closer to zero) and smaller changes in the drier values.

#### Calculation of Pore-Size Distributions

Pore-size distributions are calculated from the van Genuchten fits to measured retention points using capillary theory. Errors in the calculation of pore-size distribution may arise from assuming that a uniform surface tension between water and air applies at all phases of extraction or for the entire sample and from assuming a zero contact angle. Because pore sizes are calculated from the water-retention curves, errors in  $\psi$  will result in errors in the pore radii, with the largest errors occurring near zero pressure. Even though the pore radii do not scale directly with  $\psi$ , an error in  $\psi$  of 10 % will result in an error in the pore radius of about 10 %.

## DISCUSSION OF RESULTS

The basic question to be answered in this study is whether any systematic trends are observed in the water-retention properties of core samples taken from deposits with distinct depositional histories. Based on a sample classification scheme involving all possible combinations of degree of particle-size sorting and stratification, the significant retention properties, such as porosity, the range of pore sizes (sorting), and the air-entry pressure,  $\psi_{ae}$ , were compared to the bulk physical properties, such as median particle radius and particle-size sorting, to determine the controlling bulk factors.

### Bulk Physical Properties

The important physical attributes that could influence the water-retention properties of a core sample include textural factors, such as particle-size sorting and median particle size, and structural factors, such as stratification and the physical arrangement of grains. Particle-size statistics are used to describe textural factors, and structural properties are observed from the cores themselves. Figure 16 presents a classification scheme developed using all possible combinations of degree of particle-size sorting (Table 5) and stratification (Fig. 11). Because stratification was not examined on samples OGW-4 and SCW-1, field photographs taken at the sampling locations were studied. The channel wall where SCW-1 was sampled appeared to be weakly stratified, whereas the stratification at the sampling location of OGW-4 was difficult to discern.

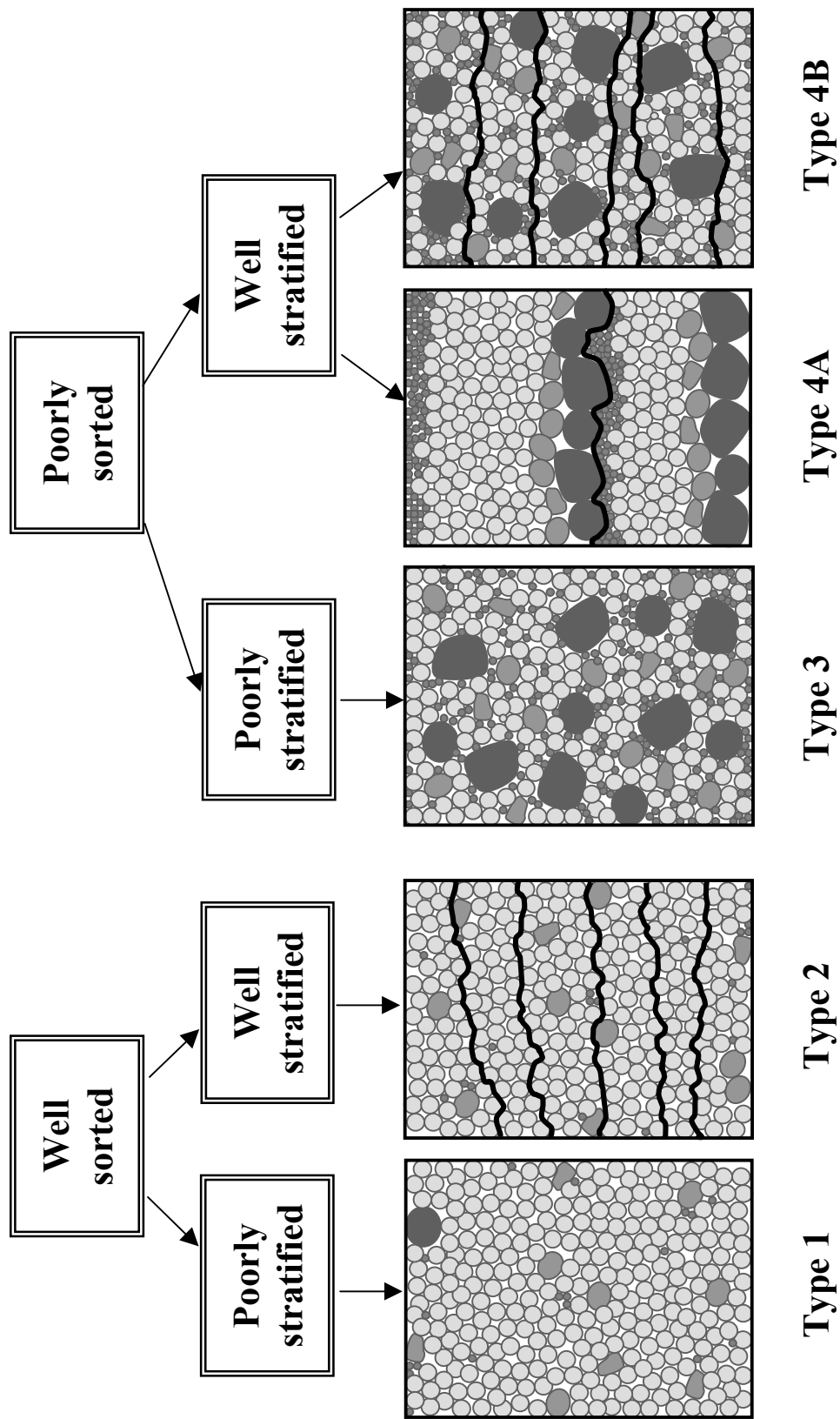


Figure 16. Sample classification scheme based on particle-size sorting and stratification.

Although none of the samples is considered well sorted by statistical limits (Folk, 1980), the samples with the lowest sorting values,  $< 2 \phi$  units, are here termed well sorted, with all others considered poorly sorted. Samples with little to no observed layering are categorized as poorly stratified and those with a significant number of layers, typically 3 or more, are considered well stratified (Table 8).

Table 8. Sample Classification Based on Particle-Size Sorting and Stratification

Sample	Particle-Size Sorting ( $\phi$ )	Number of Layers	Sorting Description	Stratification Description	Type <sup>1</sup>
OGW-1	1.28	8	Well	Well	2
OGW-2	1.67	1	Well	Poor	1
OGW-4	2.66	ND	Poor	ND	3 or 4
OGL 11.5-12	3.18	1	Poor	Poor	3
LOGW-2 82-82.5	2.63	2	Poor	Poor	3
SCW-1	2.72	(1)	Poor	(Poor)	3
SCW-2	1.55	1	Well	Poor	1
SCW-4	2.62	3	Poor	Well	4
SCF 57-57.5	2.57	8	Poor	Well	4
LSCW 58-58.5	3.15	4	Poor	Well	4

( ) indicates observation made from field photographs; ND = not determined.

<sup>1</sup>Type description refers to different combinations of sorting and stratification, as shown in Figure 16.

By this system, well-sorted samples are subdivided based on degree of stratification: poorly stratified samples are referred to as Type 1 and well-stratified samples are classified as Type 2. Similarly, poorly sorted samples are categorized as Type 3 if poorly stratified and Type 4 if well stratified. Theoretically, Type 4 can be subdivided on the basis of intralayer sorting, where Type 4A samples possess well-sorted layers and Type 4B samples have poorly sorted layers. This classification allows samples to be grouped solely on the basis of physical properties of the sediments.

From this classification scheme, the various groups might be loosely associated with either fluvial or debris-flow deposits. Because samples of Type 1 and 2 are well

sorted, they are inferred to represent fluvial materials regardless of the degree of stratification present. Type 3 samples, which are poorly sorted as well as poorly stratified, are interpreted to represent debris-flow deposits. Type 4A samples, whose individual layers are well sorted, are associated with normally graded fluvial deposits. Type 4B samples, with poorly sorted layers, are associated with debris-flow deposits.

By inferring depositional facies from this classification system, it appears that both fluvial and debris-flow deposits are represented at each wash even though distinct depositional facies are observed at the surface. Because each wash is associated with alluvial fan deposition, it is logical that both fluvial and debris-flow facies exist considering that the positions of the washes have likely shifted laterally over the fan surfaces with time, and that local reworking of fan materials could produce well-sorted (fluvial) layers even on a debris-flow dominated fan. Because few samples are classified as Type 4 and because of the difficulty of visually estimating intralayer sorting, this study does not provide enough information to determine the structural effects on retention due to grain arrangement, as hypothesized in Figure 4.

Particle-size sorting and skewness values were plotted for each sample to determine if statistics provide any indication of differences in depositional environment between each wash (Fig. 17). Because the statistics represent averages for each sample, they cannot be used to differentiate between fluvial and debris-flow deposits, which would require particle-size information from individual layers. Without the presence of layering, debris-flow samples are expected to be poorly sorted (Type 3) and fine-skewed, and fluvial samples are expected to be well sorted (Type 1). The range of particle-size

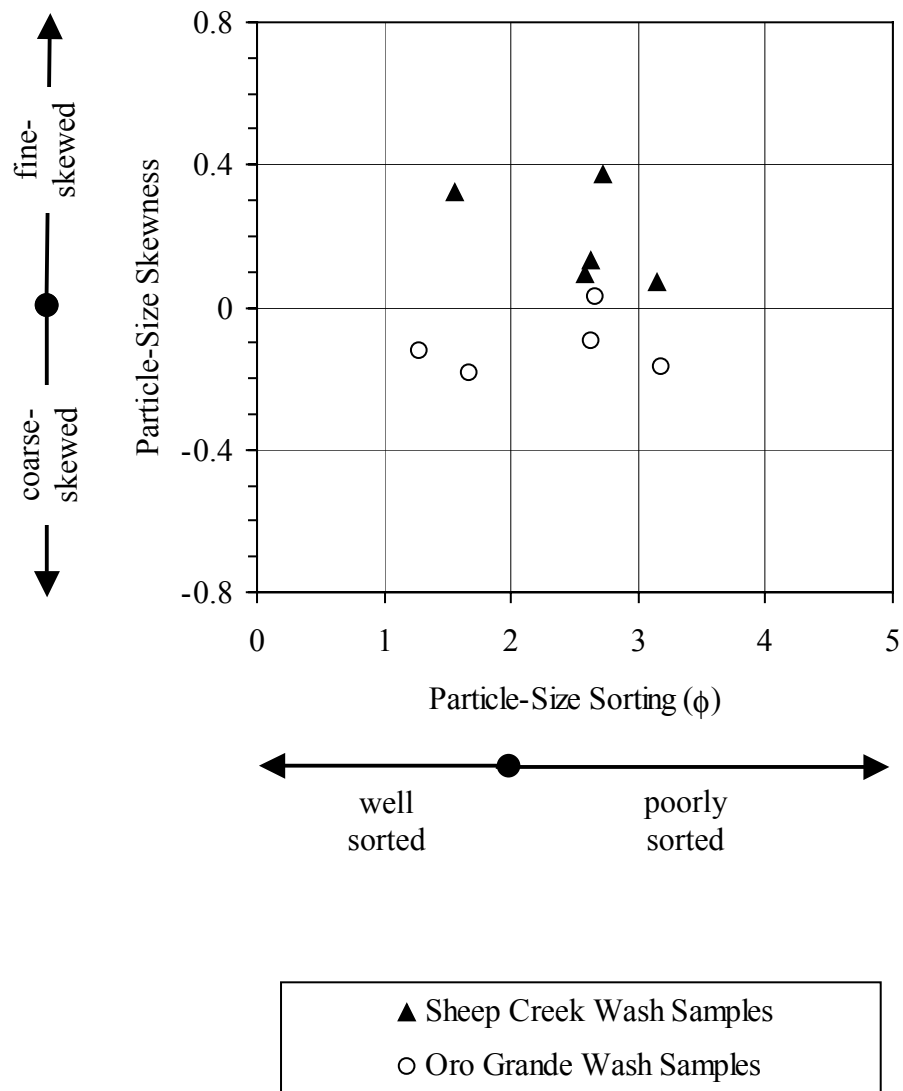


Figure 17. Comparison of particle-size sorting, in  $\phi$  units, versus particle-size skewness for samples from Oro Grande Wash and Sheep Creek Wash.

sorting values for the two washes is similar, although Sheep Creek Wash samples tend to be more finely skewed than samples from Oro Grande Wash. This observation could reflect the debris-flow nature of the deposits at Sheep Creek Wash, but the samples seem too well stratified to be of debris flow origin. Instead, the excess fine particles in the Sheep Creek Wash samples may be attributed to the high mica contents of these samples, mica being more easily weathered to fine particles during transport and after deposition than quartz and feldspar (the dominant minerals at Oro Grande Wash).

### Hydraulic Properties

The main elements that describe a water-retention curve are the air-entry pressure,  $\Psi_{ae}$ , the saturated water content,  $\theta_{sat}$ , or porosity,  $\Phi$ , and the drainage slope. Porosity includes information about the density of grain packing as related to grain sorting, shape, arrangement, and orientation. The slope of the cumulative pore-size distribution curve is comparable to the sorting value, in  $\phi$  units, determined from graphical statistics. Larger  $\phi$  values correspond to a wider range of pore sizes. According to capillary theory, the largest pores drain first. Therefore, between two samples with similar textures, the sample with the higher (less negative) air-entry pressure has more large pores.  $\Psi_{ae}$  is derived directly from the empirical curve-fit procedure, corresponding to the inverse of the parameter  $\alpha$ . For a randomly structured deposit such as a debris flow, e.g. Type 3, one could expect a lower (more negative) air-entry value than for a more regularly structured medium like a normally graded fluvial deposit, e.g., Type 4A.



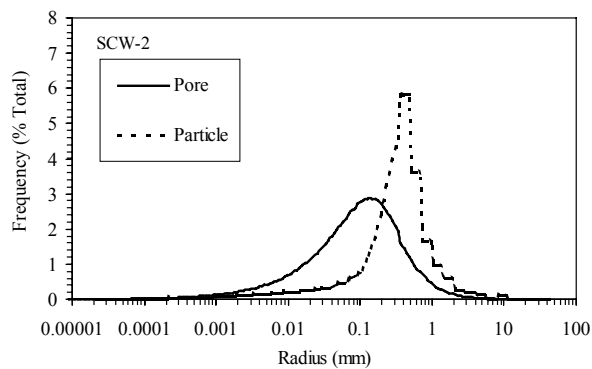
### Comparison of Bulk and Hydraulic Properties

For each sample, the pore-size distribution was computed from the measured water-retention curve and compared to the measured particle-size distribution. Pore-size and particle-size histograms for each of the four classification groups are shown in Figures 18, 19, and 20. The shape of the pore-size distributions depends on the range of the measured retention data; the starting and ending data points, in this case, porosity and residual water content,  $\theta_r$ , are particularly important in defining the range of pore sizes represented. Whereas porosity is calculated from the physical properties of bulk density and particle density, residual water content represents an optimized value, based largely on the driest measured retention points, determined by the regression algorithm of the RETC code (van Genuchten and others, 1991).

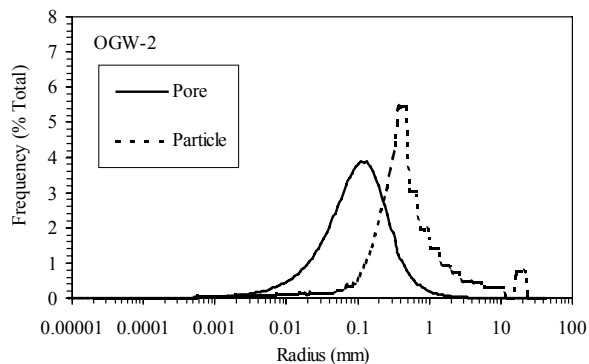
Table 9 summarizes the important physical and water-retention attributes for each sample, including median particle and pore radii, particle-size and pore-size sorting values, layering, porosity, air-entry pressure, and the ratio of the median particle radius to median pore radius,  $(PA/PO)_{\text{median}}$ . The ratio,  $(PA/PO)_{\text{median}}$ , indicates the relative shift in the median size of each distribution, approximated by the distance between the peaks in the histograms. The ratio of the particle- to pore-size mode could also have been used, but because of the slight inequality in the  $\Delta r$  interval between sieve and optical particle-size data, the modes could not be accurately determined.

Pore-size sorting and median pore radius were compared to particle-size sorting and median particle radius to determine which bulk factors control retention (Fig. 21). Pore-size sorting, or the range of pore sizes in a sample, correlates weakly with both

Type 1:  
Well sorted  
Poorly stratified



Type 1:  
Well sorted  
Poorly stratified



Type 2:  
Well sorted  
Well stratified

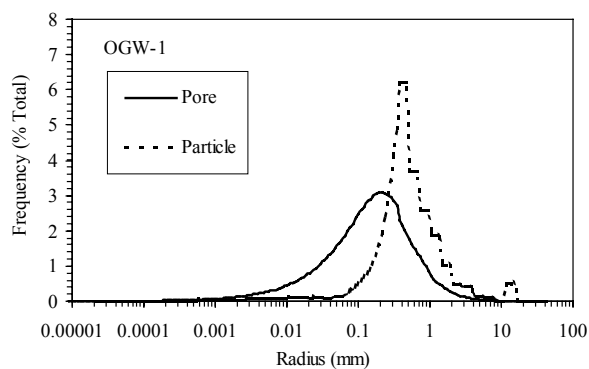
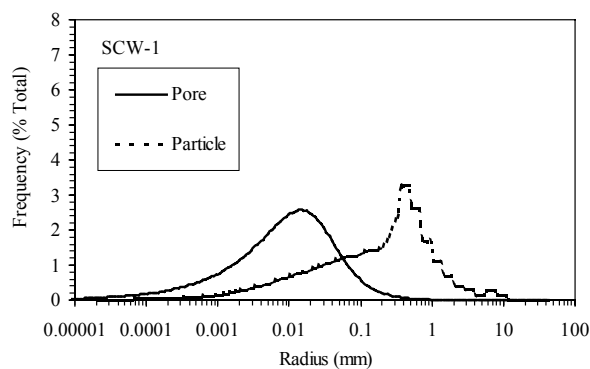
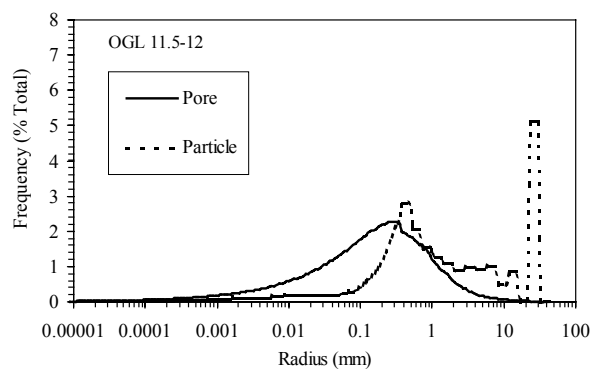


Figure 18. Pore- and particle-size histograms for samples that are well sorted in particle size and that are either poorly stratified (Type 1) or well stratified (Type 2).

Type 3:  
Poorly sorted  
Poorly stratified



Type 3:  
Poorly sorted  
Poorly stratified



Type 3:  
Poorly sorted  
Poorly stratified

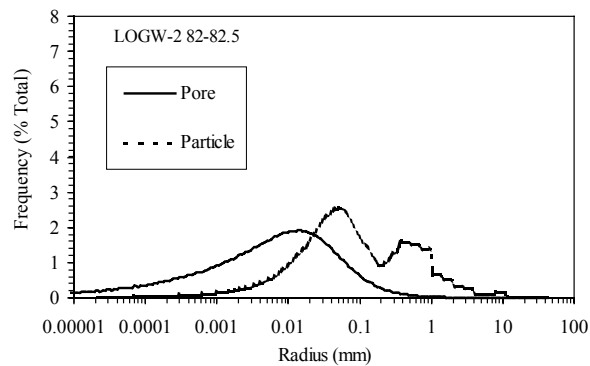
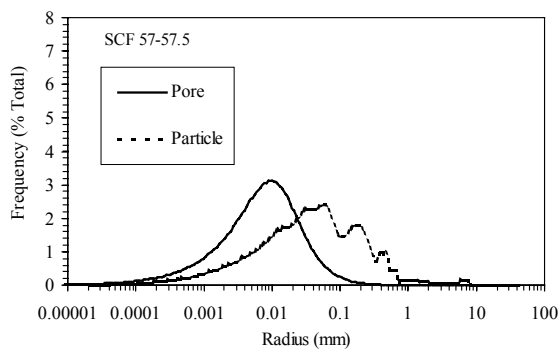
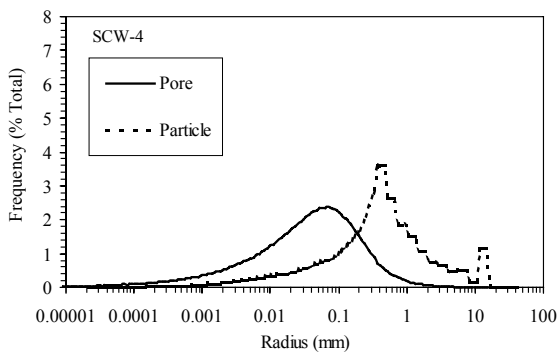
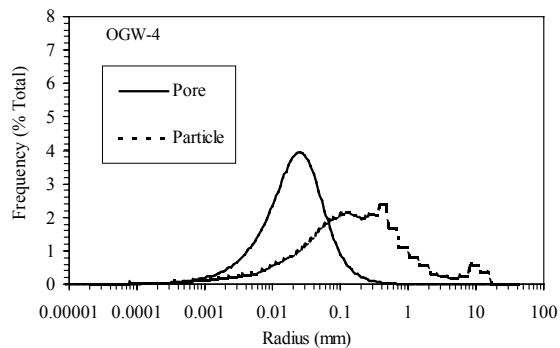


Figure 19. Pore- and particle-size histograms for samples that are poorly sorted in particle size and poorly stratified (Type 3).

Type 3 or 4:  
 Poorly sorted  
 Stratification unknown



Type 4:  
 Poorly sorted  
 Well stratified

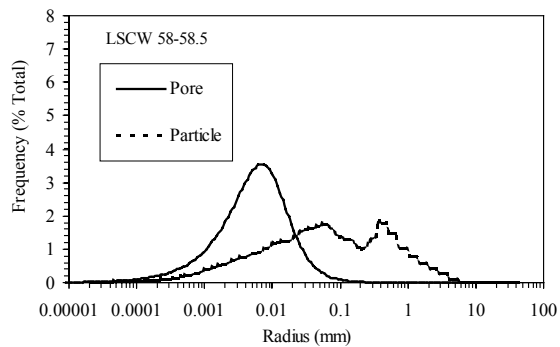


Figure 20. Pore- and particle-size histograms for samples, poorly sorted in particle size, having an unknown degree of stratification (Type 3 or 4) or displaying strong stratification (Type 4).

Table 9. Bulk Physical and Hydraulic Properties Related to Structural and Textural Trends between Samples

Sample	Bulk Physical Properties				Hydraulic Properties			
	Median Particle Radius	Particle-Size Sorting	Number of Layers	Median Pore Radius	Pore-Size Sorting	Porosity	$\Psi_{ac}$	$(PA/PO)_{median}^1$
	mm	$\phi$		mm	$\phi$		-cm H <sub>2</sub> O	
OGW-1	0.4500	1.28	8	0.1600	2.04	0.379	4.6	2.81
OGW-2	0.4330	1.67	1	0.0950	1.57	0.359	9.5	4.56
OGW-4	0.1550	2.66	ND	0.0205	1.55	0.323	44.8	7.56
OGL 11.5-12	0.9900	3.18	1	0.1700	2.90	0.287	2.6	5.82
LOGW-2 82-82.5	0.0690	2.63	2	0.0062	3.56	0.343	45.9	11.13
SCW-1	0.2500	2.72	(1)	0.0097	2.51	0.321	57.8	25.77
SCW-2	0.3700	1.55	1	0.0950	2.19	0.397	6.7	3.89
SCW-4	0.4300	2.62	3	0.0400	2.73	0.350	11.8	10.75
SCF 57-57.5	0.0370	2.57	8	0.0072	1.99	0.417	101.3	5.14
LSCW 58-58.5	0.0625	3.15	4	0.0056	1.73	0.288	154.6	11.16

( ) indicates observation made from field photographs; ND = not determined.

$^1(PA/PO)_{median}$  is the ratio of the median particle size to the median pore size.

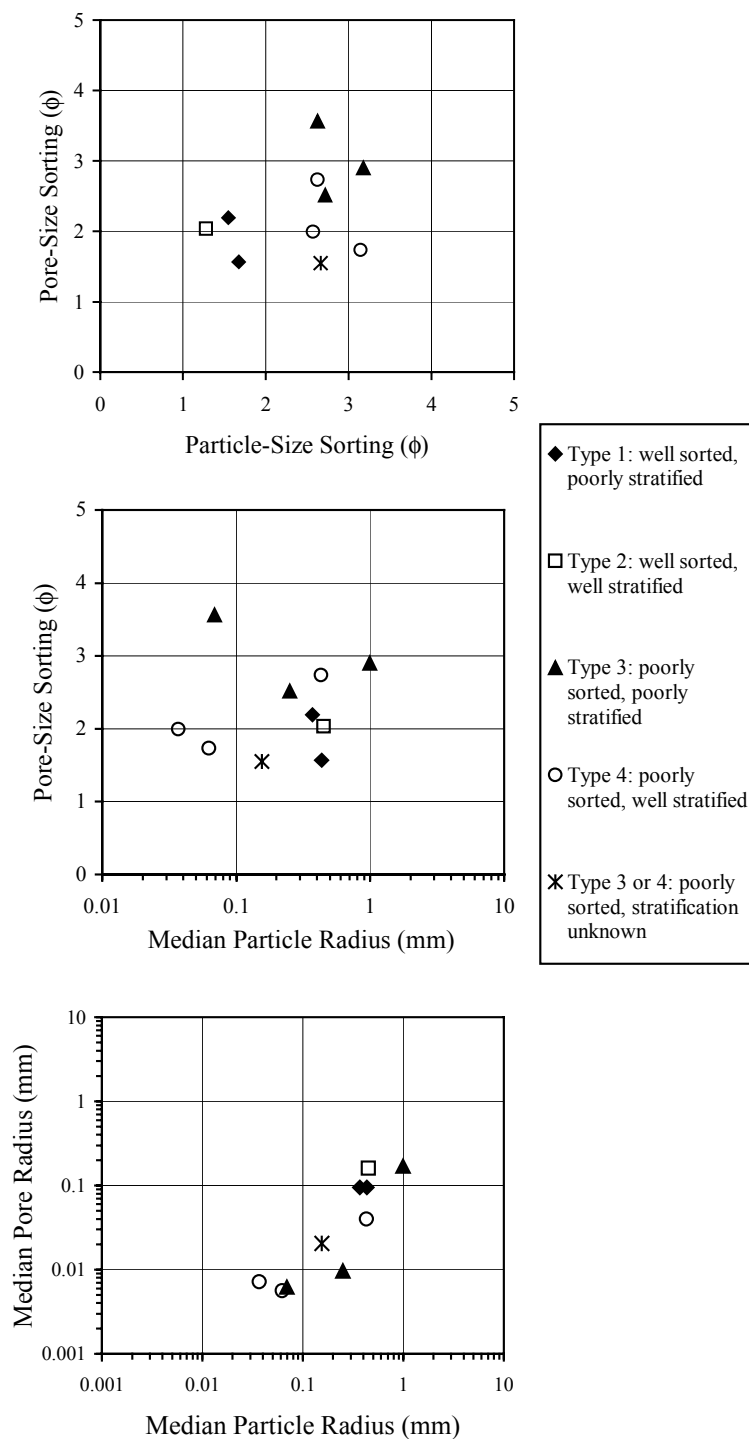


Figure 21. Trends in pore-size sorting and median pore radius. Pore-size sorting correlates poorly with particle-size sorting and the median particle radius (upper and middle diagrams). Median pore radius increases with median particle radius (lower diagram).

particle-size sorting and median particle radius. However, median pore radius shows a clear positive correlation with median particle radius. Because larger pore radii are associated with higher (less negative) values of matric pressure head according to capillary theory, the relationship between median pore and particle radius is primarily textural, as shown by the hypothetical retention curves in Figure 2. For all plots in Figure 21, the well-stratified samples, Types 2 and 4, are scattered amongst the poorly stratified samples, Types 1 and 3, suggesting that stratification has little effect on the shape of the pore-size distributions.

The ratio of the median particle and pore radius,  $(PA/PO)_{\text{median}}$ , for each sample was plotted against particle-size sorting, pore-size sorting, and median particle radius (Fig. 22). The median size was chosen because it does not include the effects of skewed or bimodal distributions. The relation between  $(PA/PO)_{\text{median}}$  and particle-size sorting shows a positive correlation, with the exception of point SCW-1, a sample with an exceptionally high value of  $(PA/PO)_{\text{median}}$  (Table 9). Well-sorted samples, Types 1 and 2, have median particle and pore radii that are close together (low  $(PA/PO)_{\text{median}}$ ), whereas more poorly sorted samples, Types 3 and 4, have the highest ratios. The increase in  $(PA/PO)_{\text{median}}$  with greater particle-size sorting values is consistent with poorly sorted samples having finer pore-size distributions because small particles tend to occupy the spaces between large particles during deposition or weathering. Because the median size is close to the mode, higher values of  $(PA/PO)_{\text{median}}$  also correspond to modes that are farther apart in the histograms. The graph of  $(PA/PO)_{\text{median}}$  versus pore-size sorting (Fig. 22) shows a poor correlation, which may be an artifact of the curve fitting procedure.





Pore-size sorting is dependent on the slope of the cumulative pore-size distribution curves, determined in part by the beginning and ending retention points, porosity and residual water content. Comparing  $(PA/PO)_{\text{median}}$  to median particle radius (Fig. 22) shows a negative correlation if the anomalous point SCW-1 is ignored; the relative shift between the median (or modal) pore and particle radii becomes smaller as the median particle radius of the sample increases.

In addition to pore-size sorting, the air-entry pressure and the porosity are important characteristics of a water-retention curve. Strong correlations are observed between  $\psi_{\text{ae}}$  and particle-size sorting as well as between  $\psi_{\text{ae}}$  and median particle radius (Fig. 23). As particle-size sorting increases (becomes worse), the absolute value of the air-entry pressure also increases. This suggests that a reduction of pore sizes occurs as more particle sizes are included in the sample mixture, with smaller particles tending to occupy the spaces between larger particles. By contrast, an increase in the absolute value of  $\psi_{\text{ae}}$  corresponds to a decrease in median particle radius. This seems to be primarily a textural effect, as illustrated in Figure 2.

For samples used in this study, porosity decreases as particle-size sorting increases (Fig. 24). As more particle sizes are added, the smallest particles will tend to occupy the voids between larger particles during deposition (or weathering), with the exception of Type 4A samples, resulting in a decrease in the porosity of the sample. The correlation between porosity and median particle radius is less distinct; however, porosity tends to decrease with increasing median particle radius. For well-sorted ideal spheres of similar packing geometries, particle size would have negligible effect on porosity.

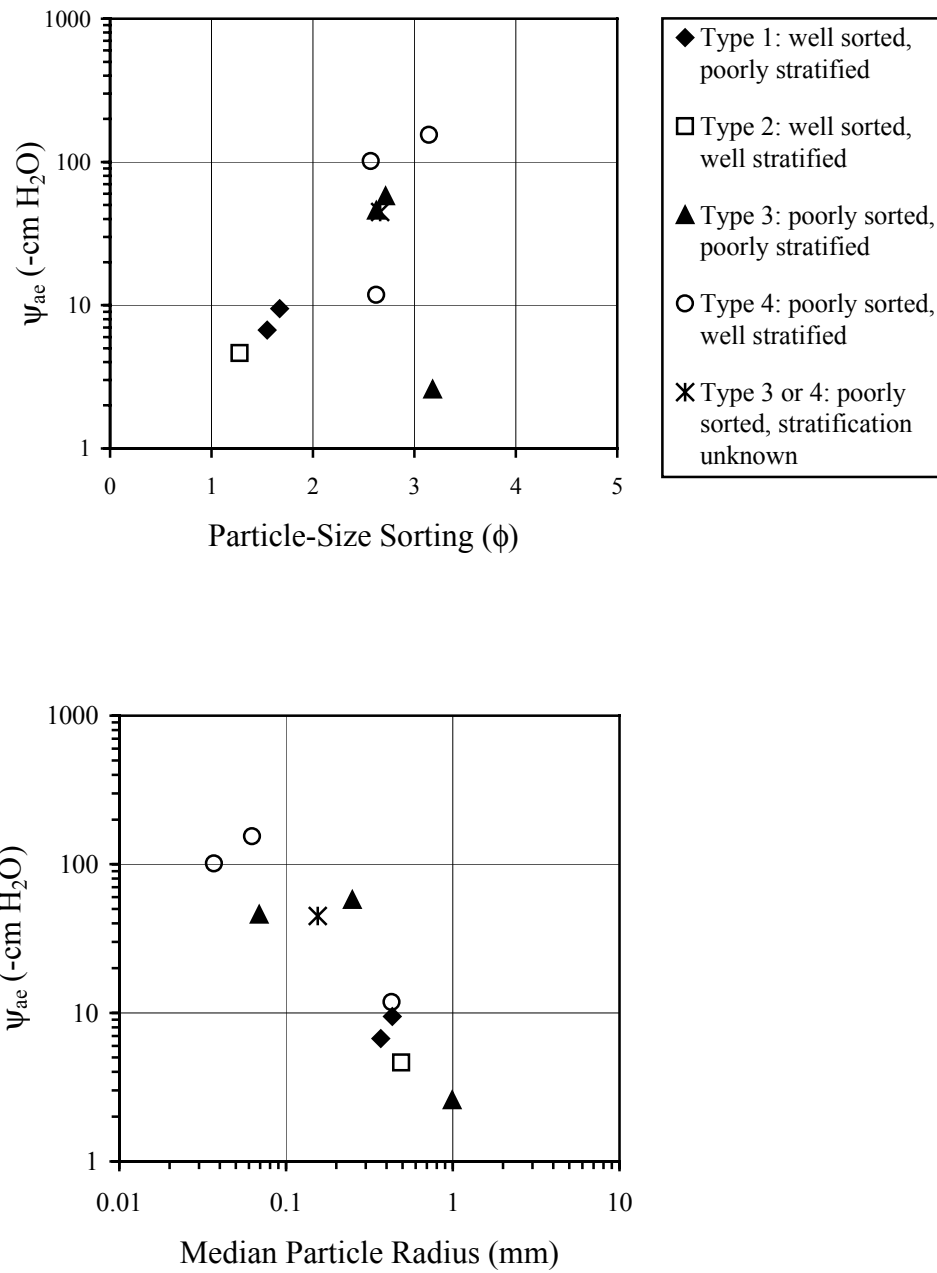


Figure 23. Trends in the air-entry pressure.  $\Psi_{ae}$  correlates positively with particle-size sorting and negatively with the median particle radius.

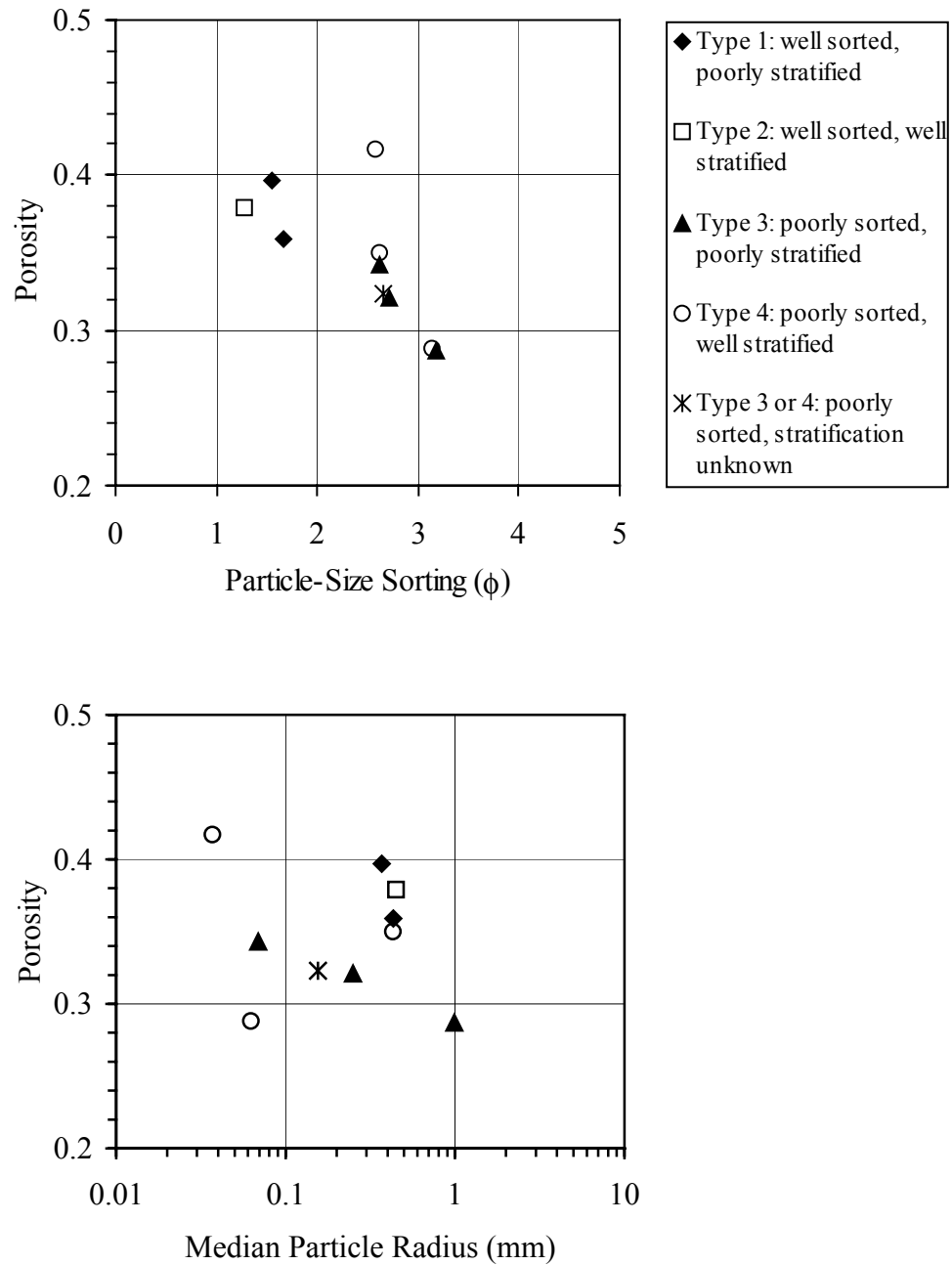


Figure 24. Trends in porosity. Porosity decreases as the number of significant particle-size classes increases. Correlation with the median particle radius is more ambiguous.

However, because sediments consist of a continuum of particle sizes and are not perfectly spherical in shape, irregularities in shape and roundness, in addition to variations in particle-size sorting, can contribute to deviations from the ideal porosity of 48 % (Graton and Fraser, 1935) for close-packed spheres. An increase in porosity with decreasing median particle radius can be explained by the increased friction, adhesion, and bridging caused by the increased ratio of surface area to packing density for finer particles (Vinopal and Coogan, 1978), in addition to variations in particle shape and sorting. Although particle-size sorting appears to be the primary control on porosity, not enough information is available to determine whether differences due to the physical arrangement of the grains affects porosity as with Types 4A and 4B (Fig. 16).

For the samples used in this study, texture appears to be the dominant control on water retention regardless of depositional environment. Median particle radius is a dominant control on median pore radius and air-entry pressure. Particle-size sorting displays strong correlations with the air-entry pressure, porosity, and to a lesser extent, with the ratio of the median particle to the median pore radius. Particle-size sorting is a more important control on porosity than median particle radius, and median particle radius rather than particle-size sorting displays a stronger control on the air-entry pressure.

Structural effects, due to grain arrangement or stratification, are not detected because they are either overwhelmed by textural effects or are insignificant for these samples. Effects due to grain arrangement could not be confirmed because there were not enough Type 4 samples to compare and because intralayer sorting was hard to

determine visually. Layering does not have a significant effect on retention for the degree of contrast observed in these cores, an observation clear from the random distribution of points between poorly stratified (Types 1 and 3) and well-stratified (Types 2 and 4) samples in Figures 21 through 24.

#### Sensitivity of Interpretations to Curve-Fit Procedure

The van Genuchten curves used in this analysis were fitted between porosity, to represent the largest pores, and optimized values of residual water content, to produce better fits to the driest measured retention points.  $\theta_r$  is dependent on the range of  $\theta(\psi)$  values measured for a particular sample. The residual water contents for samples LSCW 58-58.5, SCF 57-57.5, and OGW-4 (Table 6) are unrealistically high for sands. As a result their pore-size distributions have become artificially narrowed by limiting the range of water contents over which pore sizes are calculated, as observed from the pore-size histograms for these samples in Figures 18 through 20. SCF 57-57.5 and LSCW 58-58.5 contain higher clay percentages than the other samples (Table 4) and are the two finest samples in terms of median particle radius (Table 5). Although both of these factors could contribute to the higher  $\theta_r$  values, the limited range of the driest measured retention points has likely artificially increased the  $\theta_r$  values for these samples during the optimization procedure. Although OGW-4 is the fourth finest sample in terms of median particle radius (Table 5), the last measured  $\psi$  value of -1600 cm H<sub>2</sub>O, with an associated water content of 0.083, is higher (less negative) than the range of lowest  $\psi$  values achieved for the other samples. Therefore the high value of  $\theta_r$  for OGW-4 is likely an

artifact of the measurement technique and not associated with a physical phenomenon, such as the cessation of drainage from the sample.

To determine the sensitivity of the calculated pore-size distributions and statistics, and hence, the interpretations of results, to the curve-fit procedure, the van Genuchten (1980) function was used to fit between porosity and a zero residual water content for all samples. The parameters of this alternate curve-fit procedure are presented in Table 10. The cumulative pore-size distributions were calculated by normalizing the  $\theta(\psi)$  curves to porosity only (according to  $S = (\theta - \theta_r)/(\Phi - \theta_r) = \theta/\Phi$ , for  $\theta_r = 0$ ) and converting  $\psi$  to the predetermined pore radii, as described previously. Pore-size statistics calculated from these cumulative pore-size distributions are presented in Table 11. As a second test of sensitivity, the van Genuchten parameters for curves fit between  $\theta_{\text{sat}}$  and  $\theta_r$  optimized, and  $\theta_{\text{sat}}$  and  $\theta_r = 0$ , are presented in Tables 12 and 13, respectively. Although the goodness of fit values,  $R^2$ , were lower when  $\theta_{\text{sat}}$  was used, the general correlations between retention and bulk properties were similar to those obtained using porosity. The two cases for porosity ( $\theta_r$  optimized and  $\theta_r = 0$ ) were chosen to show how the value of  $\theta_r$  could affect the results.

By altering the way the measured retention points are fit using the van Genuchten (1980) formula, it was found that the value of pore-size sorting is highly sensitive to the curve-fit parameters. Pore-size sorting is the retention property most sensitive to the curve-fit technique. The other retention properties, such as median pore radius, porosity, and  $\psi_{\text{ae}}$ , are either unaffected or little changed by altering the curve-fit procedure.

Table 10. van Genuchten Parameters with Calculated  $\Phi$  and  $\theta_r = 0$ 

Sample	$\alpha$	$1/\alpha$	n	m	$R^2$
	$\text{cm}^{-1}$	cm			
OGW-1	0.3118	3.2	1.4867	0.3274	0.9654
OGW-2	0.1106	9.0	1.8676	0.4646	0.9918
OGW-4	0.0265	37.7	1.5625	0.3600	0.9600
OGL 11.5-12	1.0067	1.0	1.2785	0.2178	0.9716
LOGW-2 82-82.5	0.0236	42.4	1.3635	0.2666	0.9783
SCW-1	0.0194	51.7	1.4953	0.3313	0.9829
SCW-2	0.1576	6.3	1.6309	0.3868	0.9966
SCW-4	0.0934	10.7	1.4684	0.3190	0.9887
SCF 57-57.5	0.0148	67.8	1.3613	0.2654	0.9668
LSCW 58-58.5	0.0079	126.9	1.3593	0.2643	0.9757

Table 11. Pore-Size Statistics for Curve Fits Using Calculated  $\Phi$  and  $\theta_r = 0$ 

Sample	Mean Radius	Median Radius	Sorting	$C_u$	Skewness	Kurtosis
	mm	mm	$\phi$		$\phi/\phi$	$\phi/\phi$
OGW-1	0.0911	0.1200	3.10	45.2	0.26	1.16
OGW-2	0.0757	0.0880	1.90	10.5	0.21	1.14
OGW-4	0.0098	0.0120	2.73	28.4	0.22	1.16
OGL 11.5-12	0.0555	0.1250	5.18	666.7	0.37	1.15
LOGW-2 82-82.5	0.0036	0.0056	3.94	139.7	0.31	1.18
SCW-1	0.0057	0.0070	3.00	42.9	0.22	1.16
SCW-2	0.0709	0.0890	2.48	19.8	0.24	1.16
SCW-4	0.0255	0.0350	3.14	53.9	0.28	1.15
SCF 57-57.5	0.0022	0.0034	3.90	157.9	0.31	1.16
LSCW 58-58.5	0.0012	0.0018	3.93	160.0	0.30	1.16

Table 12. van Genuchten Parameters with Measured  $\theta_{\text{sat}}$  and Optimized  $\theta_r$ 

Sample	$\alpha$	$1/\alpha$	n	m	$\theta_r$	$R^2$
	$\text{cm}^{-1}$	cm			$\text{cm}^3/\text{cm}^3$	
OGW-1	0.0647	15.4	2.6337	0.6203	0.0556	0.9907
OGW-2	0.0616	16.2	2.6549	0.6233	0.0401	0.9974
OGW-4	0.0193	51.9	1.6946	0.4099	0.0483	0.9546
OGL 11.5-12	0.0772	13.0	1.8757	0.4669	0.0385	0.9791
LOGW-2 82-82.5	0.0054	186.9	2.0900	0.5215	0.0508	0.9981
SCW-1	0.0090	110.6	1.9086	0.4761	0.0355	0.9910
SCW-2	0.0618	16.2	2.2460	0.5548	0.0360	0.9918
SCW-4	0.0335	29.8	1.9069	0.4756	0.0360	0.9910
SCF 57-57.5	0.0077	129.4	2.0056	0.5014	0.0837	0.9921
LSCW 58-58.5	0.0058	172.7	2.1435	0.5335	0.0962	0.9961

Table 13. van Genuchten Parameters with Measured  $\theta_{\text{sat}}$  and  $\theta_r = 0$ 

Sample	$\alpha$	$1/\alpha$	n	m	$R^2$
	$\text{cm}^{-1}$	cm			
OGW-1	0.0641	15.6	1.8257	0.4523	0.9435
OGW-2	0.0593	16.9	2.1412	0.5330	0.9828
OGW-4	0.0193	51.9	1.6383	0.3896	0.9442
OGL 11.5-12	0.1704	5.9	1.2846	0.2215	0.9336
LOGW-2 82-82.5	0.0057	174.2	1.6699	0.4012	0.9783
SCW-1	0.0102	98.1	1.6223	0.3836	0.9788
SCW-2	0.0618	16.2	1.8712	0.4656	0.9829
SCW-4	0.0367	27.2	1.5818	0.3678	0.9821
SCF 57-57.5	0.0112	89.3	1.3785	0.2746	0.9575
LSCW 58-58.5	0.0067	149.5	1.3733	0.2718	0.9702



Changing the endpoints or range of water contents over which the fits are made significantly affects the slope of the pore-size distribution and the calculated pore-size sorting value. Whether the pore-size distribution curve is steep or gentle does not greatly influence the value of the median pore radius, which is determined by the relative location of each sample on the plots of cumulative pore volume vs. pore radii (cumulative pore-size distributions). Note that the air-entry pressures, defined as  $1/\alpha$  from the van Genuchten fits, are not altered much by the new fit procedure (Tables 6 and 10). This is likely due to the fact that the porosity is still the upper limit for water content, whereas the dry end of the curves is now driven to zero water content. Also, the median particle radius rather than particle-size sorting was previously found to be the main control on  $\psi_{ae}$ ; this correlation is not changed by the new curve-fit procedure.

The same comparisons shown in Figures 21 through 24 were made using values based on the van Genuchten function fitted between porosity and zero residual water content rather than an optimized residual water content. The plots that are most sensitive to the curve-fit technique involve the pore-size sorting value in some way (Fig. 25), with all other plots showing little change with the variation in fit. Fitting to  $\theta_r = 0$  shifts all of the pore-size sorting values to more poorly sorted values for all pore-size distributions except Type 1; this makes sense because the slope of the pore-size distribution changes and the percent saturation,  $S = (\theta - \theta_r)/(\Phi - \theta_r) = \theta/\Phi$ , varies over a wider range of water contents. As a result, pore-size sorting correlates more strongly with particle-size sorting (Fig. 25) than before (Fig. 21). This plot suggests that, as the degree of sorting in particle

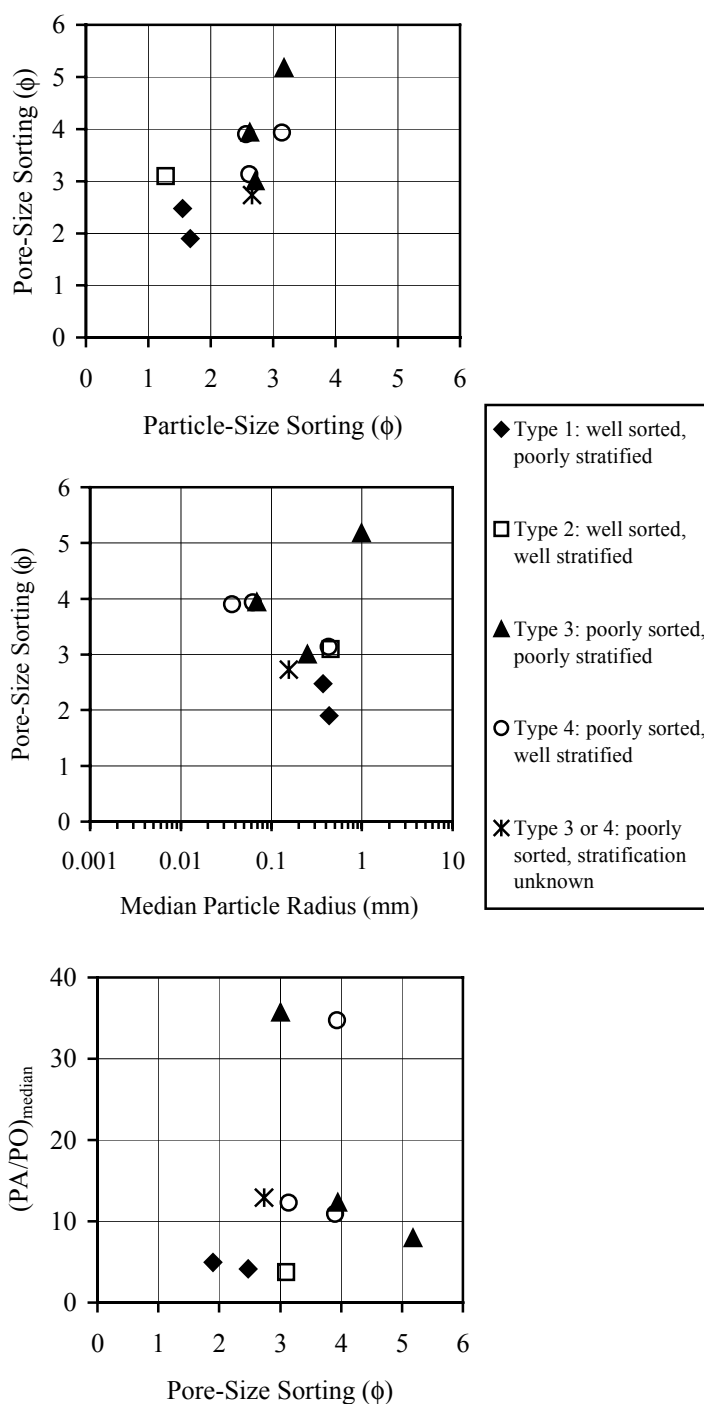


Figure 25. Sensitivity of pore-size sorting to curve-fit procedure, using calculated porosity and  $\theta_r = 0$ . Pore-size sorting shows a much stronger correlation with particle-size sorting and median particle radius when  $\theta_r = 0$ , than using  $\theta_r$  optimized (Fig. 21), but it still shows a poor correlation with the ratio of the median particle and pore radii,  $(PA/PO)_{\text{median}}$ .

sizes becomes worse (larger  $\phi$  values), there is a corresponding increase in the sorting value for pore sizes. Also by assuming  $\theta_r = 0$ , a plot of pore-size sorting versus median particle radius shows a negative correlation (Fig 25); pore sizes become better sorted as particle size increases, with the exception of one point corresponding to sample OGL 11.5-12. However, the correlation between  $(PA/PO)_{\text{median}}$  and pore-size sorting (Fig. 25) shows little improvement from before (Fig. 22) when statistics are calculated from the curves fit between porosity and zero residual water content.

#### Recommendations for Future Studies

Future studies designed to compare bulk physical properties of core samples to their measured water-retention properties would be improved by modifying the laboratory procedures used in this study. Higher apparent saturation values with less trapped air could be produced by immersing the samples to the tops of their liners in the wetting solution, vacuum saturating the samples, or flushing the samples with  $\text{CO}_2$  before saturation. This would ensure that all samples were starting from the same percent saturation (relative to porosity) during desaturation.

Dry-range retention measurements are difficult to determine, especially on large, undisturbed cores. However, the length of time for equilibration could be increased when using the filter paper method to determine matric pressure head values. Alternatively, a vapor equilibration method, such as one using a chilled-mirror humidity sensor, could be used to measure the driest points. Such methods require small representative samples of the entire core, which destroys the natural structure. The use of shorter columns would

cause faster pressure equilibration and less discrepancy in  $\psi$  between the endpoints of the samples (the  $\Delta\psi$  range over the sample length,  $L$ ), although any effects on the retention properties due to layering may be reduced.

In this study, differences in particle-size sorting between layers were not easily discerned, making it difficult to distinguish samples of Type 4A from those of Type 4B (Fig. 16). Effects on water retention due to particle arrangement were not strongly evident. Also, textural effects may overwhelm structural effects. The degree of textural contrast between layers was minimal in this study; therefore it may be necessary to study samples in which the layers have a higher degree of contrast to show the effects due to stratification. One possibility for future investigation involves first measuring retention on an undisturbed core sample, then repacking the samples and measuring retention again. Repacking could be accomplished to produce a homogeneous sample or one with very distinct, particle-size sorted layers. Because the undisturbed and disturbed packing geometries would have the same particle-size distribution, the textural effect on retention would be constant. Any differences in the curves could then be examined for structural effects.

The retention curves of undisturbed samples with random particle-size arrangements and no stratification should match, in basic character, the retention curves of samples repacked in a homogeneous fashion. Stratification of undisturbed cores could be analyzed after the measurement of retention is complete. Subsamples could be taken along the length of the cores and analyzed for particle size to help determine the type of deposit. For example, layered debris-flow samples may show uniform mean or median

particle-size profiles along the length of the cores, whereas normally graded fluvial deposits (well stratified and poorly sorted overall) may show variable profiles. The effect that the number of layers in an undisturbed core has on retention can then be compared against the single-layer random structure of the repacked cores. Alternatively, undisturbed layered cores can be compared with their repacked counterparts, in one case with size-sorted layers and in another with homogenous layers. The effects of grain arrangement could then be analyzed without the dominating influence of variations in average texture. The effects on porosity and air-entry pressure as a result of repacking could also be examined independent of textural effects.

## CONCLUSIONS

Water-retention curves were measured for 10 core samples from both Oro Grande Wash and Sheep Creek Wash in the western Mojave Desert. This study provided useful unsaturated hydraulic property information on coarse-textured media with significant gravel percentages. Hydraulic properties that are accurate and representative of the media being modeled are needed for prediction of recharge and understanding unsaturated flow mechanisms.

Water-retention properties, such as air-entry pressure, porosity, median pore radius, and pore-size sorting, were compared with various bulk physical properties, such as particle-size sorting, median particle radius, and stratification, to determine the physical factors controlling retention. Textural factors, such as median particle radius and particle-size sorting, were the main controls on the water-retention properties of the sandy sediments from these two washes, whereas structural factors showed no discernable effects. Particle-size sorting was found to be the main influence on the shape of the retention curves, in terms of porosity and the range of pore sizes. Pore-size sorting values were highly sensitive to the method of fitting the van Genuchten function to the measured retention points. Median particle radius was the main control on the air-entry values: a decrease in  $\psi_{ae}$  toward more negative values correlated with a decrease in median particle radius. Median pore radius also showed a strong positive correlation with median particle radius. The ratio of median particle radius to median pore radius was influenced mainly by the degree of particle-size sorting within the samples.

The measured retention properties of these core samples were not significantly affected by structure. Effects due to grain arrangement were not determined in this study due to the lack of data about sorting within individual layers and the small number of samples considered both well stratified and poorly sorted. Grain arrangement, as well as orientation, may be important in samples that display more distinct fluvial and debris-flow character. Stratification did not affect hydraulic properties on the core scale, at least not for the degree of textural contrast between layers that existed in the cores of this study.

Models based on textural properties alone do not always adequately predict measured retention curves. Generic  $\theta(\psi)$  or  $K(\theta)$  curves based on texture may not be appropriate in modeling unless they represent the media being modeled, because a wide range of curves is represented by a given textural class. This study provided the important relationships between various textural properties of the sediments and measured water-retention properties. The development of empirical models may need to include the relationship between median pore size and median particle size, in addition to the effect of particle-size sorting on retention. Stratification can be excluded in these models at least for samples that have weak textural contrasts between layers.

## REFERENCES CITED

- Arya, L. M., and Paris, J. F., 1981, A physicoempirical model to predict the soil moisture characteristic from particle-size distribution and bulk density data: *Soil Science Society of America Journal*, v. 45, p. 1023-1030.
- Blake, G. R., and Hartge, K. H., 1986, Particle density, *in* Klute, A., ed., *Methods of soil analysis, part I—physical and mineralogical methods (second edition)*: Madison, Wisconsin, Soil Science Society of America, Inc., Agronomy Series, n. 9, p. 378-379.
- Brooks, R. H., and Corey, A. T., 1964, Hydraulic properties of porous media: Colorado State University Hydrology Paper, n. 3, 27 p.
- Campbell, G. S., and Gee, G.W., 1986, Water potential: miscellaneous methods, *in* Klute, A., ed., *Methods of soil analysis, part I—physical and mineralogical methods (second edition)*: Madison, Wisconsin, Soil Science Society of America, Inc., Agronomy Series, n. 9, p. 628-630.
- Chandler, R. J., and Gutierrez, C. I., 1986, The filter-paper method of suction measurement: *Geotechnique*, v. 36, p. 265-268.
- Cooper, L. R., Haverland, R. L., Hendricks, D. M., and Knisel, W. G., 1984, Microtrac particle-size analyzer: an alternative particle-size determination method for sediment and soils: *Soil Science*, v. 138, n. 2, p. 138-146.
- Danielson, R. E., and Sutherland, P. L., 1986, Porosity, *in* Klute, A., ed., *Methods of soil analysis, part I—physical and mineralogical methods (second edition)*: Madison, Wisconsin, Soil Science Society of America, Inc., Agronomy Series, n. 9, p. 450-457.
- Driscoll, F. G., 1986, *Groundwater and wells (second edition)*: Saint Paul, Minnesota, Johnson Filtration Systems, Inc., 1089 p.
- Fawcett, R. G., and Collis-George, N., 1967, A filter paper method for determining the moisture characteristics of soil: *Australian Journal of Experimental Agriculture and Animal Husbandry*, v. 7, n. 24, p. 162-167.
- Folk, R. L., 1980, *Petrology of sedimentary rocks (second edition)*: Austin, Texas, Hemphill Publishing Company, 184 p.



- Gale, S. J., and Hoare, P. G., 1991, Quaternary sediments: petrographic methods for the study of unlithified rocks: London, England, Belhaven Press, 323 p.
- Gee, G. W., and Bauder, J. W., 1986, Particle-size analysis, *in* Klute, A., ed., Methods of soil analysis, part I—physical and mineralogical methods (second edition): Madison, Wisconsin, Soil Science Society of America, Inc., Agronomy Series, n. 9, p. 383-411.
- Graton, L. C., and Fraser, H. J., 1935, Systematic packing of spheres with particular reference to porosity and permeability: *Journal of Geology*, v. 43, p. 785-909.
- Greacen, E. L., Walker, G. R., and Cook, P. G., 1987, Evaluation of the filter paper method for measuring soil water suction: *International Conference on Measurement of Soil and Plant Water Status*, v. 1, p. 137-143.
- Gupta, S. C., and Larson, W. E., 1979, Estimating soil water retention characteristics from particle size distribution, organic matter content, and bulk density: *Water Resources Research*, v. 15, n. 6, p. 1633-1635.
- Hamblin, A. P., 1981, Filter-paper method for routine measurement of field water potential: *Journal of Hydrology*, v. 53, p. 355-360.
- Haverkamp, R., and Parlange, J. Y., 1986, Predicting the water-retention curve from particle-size distribution: 1. Sandy soils without organic matter: *Soil Science*, v. 142, n. 6, p. 325-339.
- Ingram, R. L., 1971, Sieve analysis, *in* Carver, R. E., ed., *Procedures in sedimentary petrology*: New York, New York, John Wiley and Sons, Inc., p. 49-67.
- Izbicki, J. A., 1999, Transition probability/Markov Chain analysis of the subsurface geology of the Victorville fan in the western part of the Mojave Desert, southern California, *in* Reynolds, R. E., and Reynolds, J., eds., *Tracks along the Mojave: Quarterly of the San Bernardino County Museum Association*, v. 46, n. 3, p. 55-64.
- Izbicki, J. A., Martin, P., and Michel, R. L., 1995, Source, movement and age of groundwater in the upper part of the Mojave River basin, California, U.S.A., *in* Adar, E. M., and Leibundgut, C., eds., *Proceedings of an international symposium on application of tracers in arid zone hydrology*, Vienna, Austria, August 22-26, IAHS-AISH Publication, n. 232, p. 43-56.
- Izbicki, J. A., Michel, R. L., and Martin, P., 1998, Chloride and tritium concentrations in a thick unsaturated zone underlying an intermittent stream in the Mojave Desert, southern California, U.S.A., *in* Brahana, J.V., Eckstein, Y., Ongley, L. K.,

- Schneider, R., and Moore, J. E., eds., Gambling with groundwater—physical, chemical, and biological aspects of aquifer-stream relations: Proceedings of the joint meeting of the XXVIII congress of the International Association of Hydrogeologists and the annual meeting of the American Institute of Hydrologists, Las Vegas, Nevada, September 28-October 2, p. 81-88.
- Klute, A., 1986, Water retention: laboratory methods, *in* Klute, A., ed., Methods of soil analysis, part I—physical and mineralogical methods (second edition): Madison, Wisconsin, Soil Science Society of America, Inc., Agronomy Series, n. 9, p. 635-662.
- Lappala, E. G., Healy, R. W., and Weeks, E. P., 1987, Documentation of computer program VS2D to solve the equations of fluid flow in variably saturated porous media: U. S. Geological Survey Water Resources Investigations Report 83-4099, 184 p.
- Lawrence, G. P., 1977, Measurement of pore sizes in fine-textured soils: a review of existing techniques: *Journal of Soil Science*, v. 28, p. 527-540.
- Lines, G. C., 1995, Ground-water and surface-water relations along the Mojave River, southern California: U.S. Geological Survey Water Resources Investigations Report 95-4189, 43 p.
- Loizeau, J. L., Arbouille, D., Santiago, S., and Vernet, J. P., 1994, Evaluation of a wide range laser diffraction grain size analyzer for use with sediments: *Sedimentology*, v. 41, p. 353-361.
- McManus, J., 1988, Grain size determination and interpretation, *in* Tucker, M., ed., Techniques in sedimentology: Oxford, England, Blackwell Scientific Publications, p. 63-85.
- Meisling, K. E., and Weldon, R. E., 1989, Late Cenozoic tectonics of the northwestern San Bernardino Mountains, southern California: *Geological Society of America Bulletin*, v. 101, p. 106-128.
- Morton, D. M., and Sadler, P. M., 1989, The failings of the Pelona Schist: landslides and sackungen in the Lone Pine Canyon and the Wrightwood areas of the San Gabriel Mountains of Southern California, *in* Sadler, P. M., and Morton, D. M., eds., Landslides in a semi-arid environment with emphasis on the inland valleys of southern California: Publications of the Inland Geological Society, v. 2, p. 301-322.

- Nagpal, N. K., Boersma, L., and Debacker, L. W., 1972, Pore size distributions of soils from mercury intrusion porosimeter data: Soil Science Society of America Proceedings, v. 36, p. 264-267.
- Nimmo, J. R., 1997, Modeling structural influences on soil water retention: Soil Science Society of America Journal, v. 61, p. 712-719.
- Ragab, R., Feyen, J., and Hillel, D., 1982, Effect of the method for determining pore size distribution on prediction of the hydraulic conductivity function and of infiltration: Soil Science, v. 134, n. 2, p. 141-145.
- Richards, L. A., 1941, A pressure-membrane extraction apparatus for soil solution: Soil Science, v. 51, p. 377-386.
- Sharp, R. P., and Nobles, L. H., 1953, Mudflow of 1941 at Wrightwood, southern California: Geological Society of America Bulletin, v. 64, p. 547-560.
- Stephens, D. B., 1996, Vadose zone hydrology: Boca Raton, Florida, Lewis Publishers, 347 p.
- Su, C., and Brooks, R. H., 1980, Water retention measurement for soils: Journal of the Irrigation and Drainage Division, Proceedings of the American Society of Civil Engineers, v. 26, n. IR2, June, p. 105-112.
- van Genuchten, M. Th., 1980, A closed-form equation for predicting the hydraulic conductivity of unsaturated soils: Soil Science Society of America Journal, v. 44, p. 892-898.
- van Genuchten, M. Th., Leij, F. J., and Yates, S. R., 1991, The RETC code for quantifying the hydraulic functions of unsaturated soils: Ada, Oklahoma, U.S. Environmental Protection Agency, EPA/600/2-91/065, 85 p.
- Vinopal, R. J., and Coogan, A. H., 1978, Effect of particle shape on the packing of carbonate sands and gravels: Journal of Sedimentary Petrology, v. 48, n. 1, p. 7-24.
- Weldon, R., 1985, Implications of the age and distribution of the late Cenozoic stratigraphy in Cajon Pass, southern California, *in* Reynolds, R. E., ed., Geologic investigations along Interstate 15; Cajon Pass to Manix Lake, California: Redlands, California, San Bernardino County Museum, p. 59-68.
- Wentworth, C. K., 1922, A scale of grade and class terms for clastic sediments: Journal of Geology, v. 30, n. 5, p. 377-392.